Study of the gas phase composition of plasma produced from N2/O2 mixtures

Yagci, G.

Award date:
2006

Eindhoven University of Technology
Department of Applied Physics
Equilibrium and Transport in Plasmas

Study of the gas phase composition of plasma produced from N_2/O_2 mixtures

Göksel Yağcı

August 2006 ETP 06 – 05

Under supervision of:
Ir. R.A.B. Zijlmans
Dr. R.A.H. Engeln

Graduation professor:
Prof. dr. ir. D.C. Schram

Abstract

An expanding thermal plasma, operated on argon, is used to dissociate mixtures of N_2 and O_2. The particles produced in the plasma interact with each other both in the gas phase and at the walls of the plasma reactor. It turns out that molecules like NO, N_2O and NO_2 are formed. The goal of this project is to determine the contributions of both types of interactions to the total chemistry, leading to these new molecules.

The conversion of N_2 and O_2 into NO, NO_2 and N_2O is investigated by varying the ratio of admixed flows of N_2 and O_2, keeping the total flow constant. For all the different conditions studied, the concentrations of the stable molecules in the plasma are determined with a mass spectrometer. An absolute calibration procedure for this mass spectrometer is presented, which enables to measure the concentrations of the various stable molecules in the plasma within an accuracy of 10 %.

At admixed flow fractions of $\phi(O_2)/\phi(O_2 + N_2) > 95$ %, the observed concentrations of NO can be explained with only gas phase interactions. At lower fractions of admixed O_2, surface interactions must be dominant.

At low fractions of the admixed O_2: $\phi(O_2)/\phi(O_2 + N_2) < 5\%$, no NO is observed at all, when the total pressure in the plasma reactor is higher than 20 Pa. Increasing the admixed O_2 results in a quadratic increase of the NO density as a function of the admixed O_2 flow. At the same time, a peak in the N_2O density is observed for $\phi(O_2)/\phi(O_2 + N_2) < 5\%$. This can be explained by assuming that N_2O is formed at the reactor walls and NO is formed by a dissociation of N_2O by O atoms in the gas phase.

The threshold behavior of NO at low fractions of admixed O_2 disappears when the pressure is reduced, but the peak in the N_2O density does not change significantly. This indicates that an extra gas phase destruction mechanism of NO occurs, most likely $N + NO \rightarrow N_2 + O$, which is less efficient at lower pressures.

The maximum partial pressure of NO is found to be a fraction of 4% of the partial pressure of $N_2 + O_2$, not strongly dependent on the pressure and admixed total flows of N_2 and O_2. This indicates that a balance between NO formation reactions, both in the gas phase and at the walls of the reactor, and dissociation reactions, in the gas phase, is present.

Contents

Chapter 1

Introduction

Plasmas are widely used in many industrial applications. They exhibit a high chemical reactivity, which can be used for deposition and etching of thin functional layers and surface modification. Although plasmas have been studied widely, there is still a lack of fundamental data on the details regarding plasma-surface interactions.

In this report, plasmas created from a relatively simple gas mixture, N_2 and O_2, are studied in order to investigate the contributions of gas phase reactions and surface reactions.

1.1 General applications

Two applications of plasmas, in which surface reactions play an important role are chemical vapour deposition and fusion plasmas.

Chemical vapor deposition (CVD) [1] is a process that is often used in the semiconductor industry for the deposition of thin films. A substrate is exposed to a volatile precursor, that forms the desired functional layer on a substrate. Plasma enhanced chemical vapor deposition (PECVD) is a CVD process that uses a plasma to improve the chemical reaction rates of the precursors. PECVD processing allows deposition at lower temperatures, which is often critical in manufacturing semiconductors.

Fusion may become an important energy source in the future. One of the main challenges in the fusion research is to control the erosion of the surfaces of a tokamak during operation. Therefore, a lot of effort is put in understanding the details of the plasma-surface interactions in a fusion plasma. See for example: [2].

1.2 Plasmas containing N_2 and / or O_2

The examples mentioned above are based on relatively complex plasmas. Below, some examples of the application of plasmas containing N_2 and / or

O_2 are given.

1.2.1 Sterilization

An oxygen plasma can be used for sterilization of medical equipment. The low temperature of the used plasma makes it favorable to treat polymer based medical equipment, like an endoscope. Therefore it is a good alternative for conventional sterilization systems.

The removal or inactivation of bacteria and spores from medical equipment can also be achieved by means of a plasma. In [3] measurements on an Ar/O_2 plasma and N_2/O_2 plasma with different fractions of O_2 are discussed. Three basic mechanisms are presented that contribute simultaneously to the inactivation of bacteria in a plasma environment:

1. Direct destruction of the genetic material of spores by UV irradiation.
2. Erosion of the spores, through photon-induced desorption, which results from UV-photons breaking chemical bonds in the micro-organism that leads to the formation of volatile compounds.
3. Erosion of the spores, molecule by molecule, through etching. Etching results from the adsorption of reactive species from the plasma on the micro-organism with which they subsequently undergo chemical reactions to form volatile components. In certain cases, etching is enhanced by UV-photons.

1.2.2 Cleaning of exhaust gases

Another area where N_2/O_2 plasmas are encountered is cleaning of exhaust gases from the combustion of fossil fuels. NO_x is known to have harmful contributions to acid rain. Already some methods exist for removing NOx from exhaust gases (deNOx), like injection of ammonia into flue gas streams to chemically reduce NO_x. This is usually applied in combination with a catalyst, to convert NO to NO_2 [4], which is more soluble in specific solutions and can be removed easily. Also ozone can be injected to convert NO and NO_2 to N_2O_5 which is even more soluble. However these technologies transfer the pollutants from one system to another. That is why there has been an increasing research in deNOx using electrical discharges, see for example [5] and [6]. Besides radicals, ions and electrons seem to have a direct function in the reaction mechanisms leading to the dissociation and formation of NO_x.

1.3 This project

In the project, described in this report, N_2 and O_2 containing plasmas are studied, by means of mass spectrometry. An argon plasma is created by

means of a cascaded arc. An intense DC discharge is created in a small volume of argon gas, which expands into a vacuum chamber. The gases N_2 and O_2 are injected into the vacuum chamber and are dissociated by interacting with Ar^+ ions from the plasma. The produced atoms flow further downstream into the vacuum chamber, where they can in principle interact with each other. Because the vacuum chamber is kept typically at a pressure lower than 1 mbar, the chances for three-particle-interactions resulting in new types of stable molecules are negligible. Therefore a significant fraction of the produced atoms reaches the walls of the reactor, where surface reactions take place, and new types of molecules are created.

By measuring the concentrations of stable molecules, pathways for formation of the molecules can be deduced. Mass spectrometry is a technique which allows to measure concentrations of different molecules simultaneously and makes it therefore well suited to use as a diagnostic tool in our setup.

1.3.1 Goals

The goal of this research is to determine the most relevant reactions in these kind of plasmas. By identifying all important gas and surface reactions, a model can be made in future research on these type of plasmas.

1.3.2 Brief outline

First the plasma dynamics and kinetics of the system are briefly described. Then the used setup is described, followed by the Expanding Thermal Plasma (ETP) technique, which is used for our measurements. In the next section the mass spectrometer and its absolute calibration will be discussed followed by principles of this diagnostic tool. Then the measurements on N_2 and O_2 containing plasmas will be given. Finally the conclusions will be given.

Chapter 2

Plasma dynamics and kinetics

In this section, the working principles of the expanding thermal plasma are discussed in terms of plasma production, dissociation of injected gases, transport of plasma-produced radicals and association of the radicals into new types of molecules.

2.1 Reaction rates

All the different species in the plasma collide and interact with each other. A fraction of all the collisions between particles results in the production of new types of molecules or atoms. For example, the reaction:

$$A + B \rightarrow C, \tag{2.1}$$

with A, B and C representing arbitrary types of species, the production rate for C is

$$\frac{d[C]}{dt} = k[A][B] \tag{2.2}$$

In which A, B and C are given in densities [m^{-3}] and k [m^3s^{-1}] is the rate coefficient. This rate coefficient can be described by the Arrhenius equation, and depends on the temperature, activation energy and the type of the molecule:

$$k = A\left(\frac{T}{T_{ref}}\right)^n \cdot e^{(-E_a/k_B T)}, \tag{2.3}$$

where k is the rate coefficient [m^3s^{-1}], A [m^3s^{-1}] the frequency factor or attempt frequency, which indicates how many collisions between reactants have the correct orientation to lead to the products, E_a [J] is the activation energy, k_B [J/K] the Boltzmann constant, T [K] the temperature and T_{ref} a reference temperature (usually 300 K).

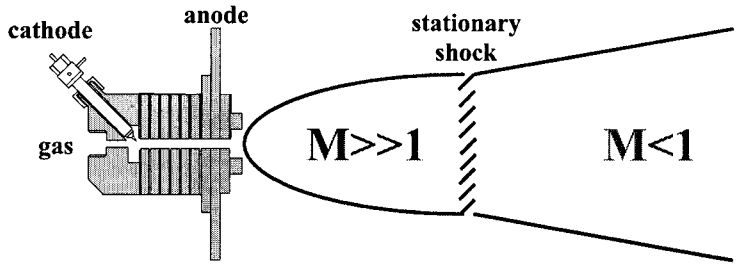

Figure 2.1: A sketch of the cascaded arc, in which the plasma is created, and the expansion of the plasma into the reactor, first supersonically, and after the shock subsonically.

2.2 Plasma creation

An argon plasma is produced by means of a cascaded arc [7]. The produced plasma expands into a vacuum vessel. This is sketched in figure 2.1.

The working gas (in this case argon) is fed through the arc channel, where a DC discharge is sustained between cathode and anode, producing Ar^+ ions and electrons. The current through the arc channel is typically 50 - 75 A. The created plasma is so intense, that in the center of the arc channel the plasma is close to LTE (the temperature of the heavy particles T_h, is approximately equal to the electron temperature T_e) at a temperature of 1 eV. The current through the arc determines the fraction of produced Ar^+ ions. M.A. Blauw et. al. [8] have determined that for a current of 40 A and 75 A, respectively 10 % and 15 % of the Ar flow through the arc is ionized.

2.3 Production of radicals

As there is no power input anymore in the process chamber, the plasma is recombining and the enthalpy is carried out in the expansion by the ions or the atomic radicals. After the stationary shock the temperature is determined by a balance between the power input to the arc and heat conduction to the walls. For Ar at typical conditions, the electron temperature in the expansion decreases to 0.1-0.3 eV and slowly decays down to about 450 to 600 K near the surface for the heavy particles. The electron density downstream is 10^{18} m^{-3}. The electron temperature is too low for electron induced dissociation or excitation processes to play a significant role.

The plasma expands in the process chamber. Due to the high pressure difference between plasma channel (usually 0.4 bar) and the process chamber (typically 20 Pa) a supersonic expansion is created followed by a stationary shock and a subsonic expansion towards the other end of the process chamber.

The gases N_2 and O_2 are injected directly into the vacuum vessel and

are mixed efficiently with the expanding plasma. There they interact with the Ar^+ ions and electrons via charge transfer and subsequent dissociative recombination reactions, creating N and O atoms:

$$\begin{aligned} Ar^+ + N_2 &\rightarrow Ar + N_2^+, && (2.4)\\ N_2^+ + e &\rightarrow N + N + e, && (2.5)\\ Ar^+ + O_2 &\rightarrow Ar + O_2^+, && (2.6)\\ O_2^+ + e &\rightarrow O + O + e. && (2.7) \end{aligned}$$

Furthermore, a produced N atom is capable of dissociating an O_2 molecule via:

$$N + O_2 \rightarrow NO + O \qquad (2.8)$$

The rate coefficients of these reactions can be found in appendix A.

2.4 Transport of radicals and molecules

After the radicals are created in the expansion, they flow into the background of the vacuum vessel and onto the walls of the reactor through convection and diffusion. In figure 2.2 a schematic view is given of both mechanisms.

2.4.1 Diffusion

The diffusion time τ_D, which is the time in which a particle diffuses about 0.1 m($\simeq$0.5 times the radius of the vessel) out the central flow can be estimated as:

$$\tau_D \sim \frac{{L_D}^2}{D} \sim \frac{\frac{R^2}{4}}{D}. \qquad (2.9)$$

Here $L_D \sim$ R/2, R [m] is the radius of the plasma vessel and D [m^2/s] the diffusion coefficient:

$$\begin{aligned} D \simeq v\lambda &\simeq \sqrt{\frac{kT}{m}}\frac{1}{n\sigma} \simeq \sqrt{\frac{1.6\cdot 10^{-19}\hat{T}_e}{A/6\cdot 10^{23}}}\cdot\frac{1.6\cdot 10^{-19}\hat{T}_e}{p\sigma}\\ &\simeq 5\cdot 10^{-17}\frac{\hat{T}_e^{1.5}}{A^{0.5}p\sigma} \qquad (2.10) \end{aligned}$$

In the case of argon, v is the thermal velocity of a (Ar) neutral particle [m/s], λ the mean free path [m], A the atomic number $\simeq$ 20, σ is the cross section of interactions with Ar neutral interactions = 1$\cdot$ 10^{-19} m^2, $\hat{T}_e$ the electron temperature in [eV] $\simeq$ 0.2, R$\simeq$ 0.1 m, then D $\simeq$ 0.5m^2/s and then $\tau_D \simeq$ 5 ms at p = 20 Pa.

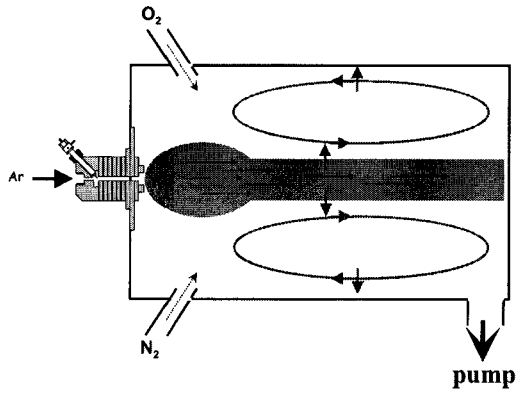

Figure 2.2: A sketch of the radical transport to surface. The radicals diffuse out of the main stream. Then the radical follows the convection pattern indicated with the ovally lines. Near the surface the radicals diffuse to the surface.

2.4.2 Convection

In figure 2.3, a schematic view and the result of a Monte Carlo simulation [9], are given of the convection pattern of the particles in the plasma vessel. The lines represent the streamlines of the particles and the color represent the velocity of the particles. From the simulation, the velocity of particles near and parallel to the surface is found to be about 200 m/s. We define a convection time τ_{conv} as the average time for a particle to reach the surface through convection, assuming that within approximately 5 cm from the surface all radicals diffuse to the surface. The convection time $\tau_{conv} \approx 1$ ms.

2.4.3 Residence time

The average time that the injected species circulate in the vacuum vessel is expressed by the residence time:

$$\tau_{res} = \frac{V \times p/kT}{\phi_{gas}} \tag{2.11}$$

with ϕ_{gas} expressed in (molecules/s). In our system, with typical conditions of p=20 Pa, T=450K and typical flows of 5000 sccm (=$2.1 \cdot 10^{21}$ particles/s), the residence time $\tau_{res} \approx 1$ s. Because τ_D and τ_{conv} are much smaller than τ_{res} we conclude that all radicals reach the surface before they are pumped out of the system.

2.4.4 Recirculation

As is clear from figure 2.3, particles present in the background of the vacuum vessel, can easily recirculate into the plasma expansion again, before they

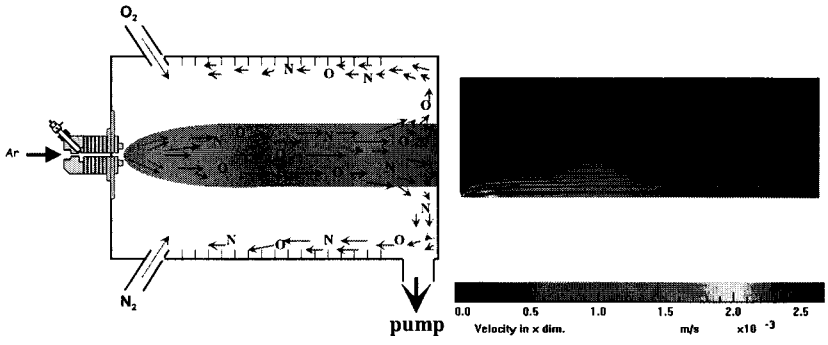

(a) Schematic view (b) Birdcode simulation

Figure 2.3: In a) a schematic view is given of an Ar plasma with injected N_2 and O_2 in the background. The radicals follow a flow indicated by the arrows. If they are not absorbed at the surface, they will recirculate. In b) a simulation with Birdcode is given of the velocities.

are pumped away. This implies that new species formed at the surfaces of the vessel can be dissociated again in the plasma expansion by Ar^+ ions or different types of radicals.

2.5 Plasma chemistry

The plasma chemistry can be divided into two types of reactions: surface reactions and gas phase reactions.

2.5.1 Gas phase

For radicals to recombine into a new, stable specie in the gas phase, usually a spectator particle is necessary to compensate for an excess of energy or impulse in the recombination process. This can be expressed as:

$$A + B + M \rightarrow AB + M, \tag{2.12}$$

where A an B represent radicals, AB the stable molecule of interest and M the spectator particle. The measurements discussed in this report are performed at relatively low pressures (less than 1 mbar). Typical rates of 3 particles reactions are lower than 10^{-44} m^6/s^{-1}. Therefore 3-particle interactions become negligible and therefore association of radicals into new, stable molecules occurs most likely at the surfaces of the reactor. In that case the surface acts as the third particle.

2.5.2 Surface interactions

Radicals can interact with each other at a surface according to two mechanisms: Langmuir-Hinshelwood and Eley-Rideal. In figure 2.4 these mecha-

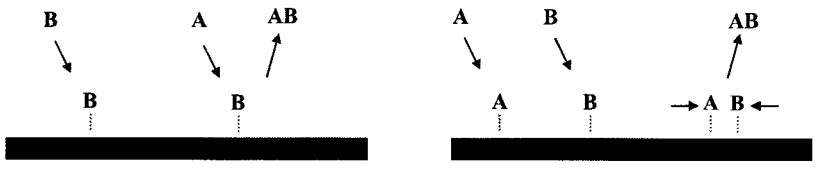

(a) Eley-Rideal (b) Langmuir-Hinshelwoord

Figure 2.4: Sketch of the Langmuir-Hinshelwood and Eley-Rideal mechanisms.

nisms are illustrated.

- In the Lamgmuir-Hinshelwood (L-H) mechanism two adsorbed molecules or atoms recombine and form a new molecule.
- In the Eley-Rideal (E-R) mechanism a molecule or atom from the gas phase directly picks up a radical or molecule that is adsorbed on the surface.

Chapter 3

Setup

In this chapter, the experimental setup is described, together with the installed diagnostics: mass spectrometry and tuneable diode laser absorption spectroscopy. This setup is named **PLEXIS**, which is short for: **PLasma EXpansion in Interaction with Surfaces.** In figure 3.1, PLEXIS is sketched.

For the production of the plasma, a cascaded arc is used, which is sketched on the left in figure 3.1. In the DC cascaded arc plasma a sub-atmospheric (typically 0.4 bar) plasma is created with a power of around 5 kW. The cascaded arc source consists of a 4 mm diameter narrow channel of 5 water cooled insulated copper plates with a total length of 30 mm. The copper plates are at floating potential. The last plate acts as the common anode for the discharge. A gas flow is admitted to the channel and a dc current is drawn from the three cathodes to the grounded anode producing the plasma. In the case of an expanding Ar plasma, the plasma source emanates a partially ionized (10-15%) Ar flow.

The plasma expands into a chamber, which is pumped down to a pressure between 1 and 1000 Pa by means of two vacuum pump series: one at the side of the substrate and one close to the cascaded arc. The first roots pump at the substrate side has a capacity of 2590 m^3/h (Edwards, EH2600). This pump is backed up by another roots pump with a capacity 500 m^3/h (Pfeiffer, WKP500), followed by a rotary vane pump with a capacity of 80 m^3/h (Edwards, E2M80). The roots pump at the arc side has a capacity of 2150 m^3/h (Pfeiffer, WKP2000). This pump is backed up by another roots pump with a capacity 500 m^3/h (Pfeiffer, WKP500), followed by a rotary vane pump with a capacity of 60 m^3/h (Pfeiffer, UNO 060A). The capacity of roots pumps are independent of the gas species. The pressure in the process chamber is measured with a barotron (MKS).

In the expansion of the plasma, N_2 and O_2 can be injected separately. In table 3.1 the used mass flow controllers with their corresponding gas and flow range are given.

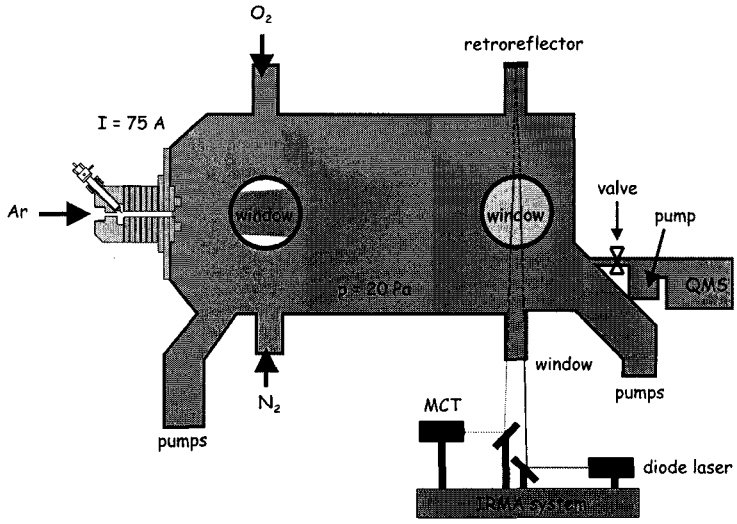

Figure 3.1: Schematic view of Plexis. The mass spectrometer and TDLAS are also sketched in the figure.

Table 3.1: Mass flow controllers.

gas	flow range (sccm)
Ar	0-5000
N_2	0-500
N_2	0-5000
O_2	0-1800

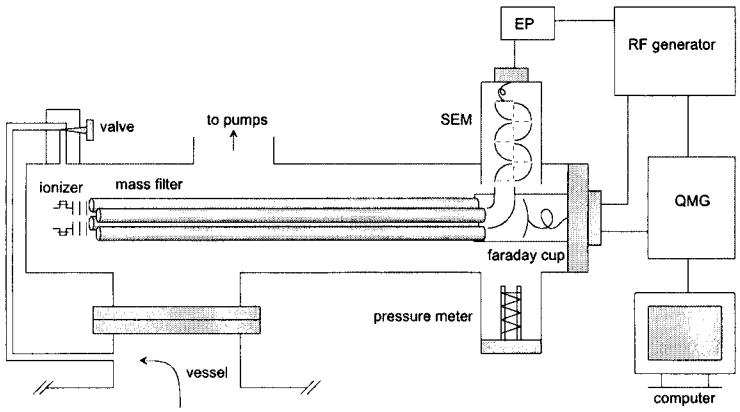

Figure 3.2: Schematic view of the Quadrupole mass spectrometer. SEM is a secondary electron multiplier, EP is a preamplifier and QMG is the control unit.

3.1 Diagnostics

The quadrupole mass spectrometer is used for all measurements as a residual gas analyzer: the stable molecules in the vacuum chamber are probed. Also a Tuneable Diode Laser Absorption Spectroscopy diagnostic is setup is used, which is called IRMA [10]. IRMA is used to calibrate the mass spectrometer for a few types of gases.

3.1.1 Quadrupole Mass Spectrometer

In this section the components of the mass spectrometer will be described. The details and working principle are presented in chapter 4.

A mass spectrometer (Balzers) consists of an ionizer, a mass filter and a detector, as shown in figure 3.2. The valve (UDV 035) regulates the gas flow from the vessel to the mass spectrometer. In the ionizer (Ion source supply IS 420, cross beam ion source) the gas is ionized. The ions are selected on their mass to charge ratio in the quadrupole mass filter (QMA 430, max 200 amu). The RF voltage used for the filtering is produced by the RF generator (QMH 400-5). The detection of the ions occurs with the Faraday cup or the secondary electron multiplier (SEM 217, power supply HV 420). Their signals are amplified by the preamplifier (EP 112) and are sent to the control unit (QMG 421C) for analysis to the computer. The mass spectrometer unit is pumped down to a pressure in the range of 10^{-5} to 10^{-9} mbar with two vacuum pumps in series: a turbo pump (TPU 180H, 180 l/s, control unit TPC 380) and a rotary vane pump (Edwards, 3 m^3/h). The pressure is measured with an ionization pressure meter (IMR 325). This ionization pressure meter is gas dependent and is calibrated for nitrogen, so for other gases a correction has to be made. To obtain the real pressure in

Table 3.2: relative sensitivities for the ionization pressure meter

Gas	Ar	N_2	O_2	NO	N_2O	CO_2	H_2O
relative sensitivity R	1.3	1	0.87	1.15	1.2	1.4	1.1

the mass spectrometer, the measured pressure has to be multiplied with the correction factors. These corrections factors are called *Relative sensitivity* R and are given in table 3.2.

3.1.2 Tuneable diode laser absorption spectroscopy

Infrared tunable diode laser absorption spectroscopy (TDLAS) can be applied to measure the concentration of species as methane, nitrous oxide and water in a gaseous mixture. The detection limit of the TDLAS system is very good (order of $10^{17}m^{-3}$), because of the strong absorption lines of several types of molecules in the infrared. Apart from the concentration, it is also possible to determine the temperature of the gas under observation. In this study this technique is used to calibrate the mass spectrometry on the absolute densities determined with TDLAS for NO and N_2O.

Working principle

A basic TDLAS setup consists of tunable diode laser light source, imaging optics and a detector. The emission wavelength of the tunable diode laser is tuned over an absorption lines of a molecule present in the laser beam, by controlling the current and temperature of the diode. The transmitted light is detected by a MCT detector, and the concentration of the molecule of interest is calculated from the absorbed light, as described below.

Concentration measurement

The focus here is on a single absorption line in the absorption spectrum of the species of interest. To start with, the wavelength of a diode laser is tuned over an absorption line and the intensity of the transmitted radiation is measured. The transmitted intensity can be related to the concentration of the species present by the *Beer-Lambert* law, which states that when light passes through an absorbing medium, its intensity decreases according to:

$$I(\nu) = I_0(\nu)e^{-\kappa(\nu)L} \tag{3.1}$$

where $I(\nu)$ is the transmitted intensity, $I_0(\nu)$ is the incident intensity, $\kappa(\nu)$ frequency dependent absorption coefficient and L the total absorption path length. The integrated absorption coefficient over the frequency is linked to the total density of the absorbing species N under consideration:

$$\kappa_\nu = \int \kappa(\nu)d\nu = N \int S(T)d\nu \tag{3.2}$$

Where *S(T)* is the line strength of the ro-vibrational transition at temperature *T*. It should be noted that the line strength used here includes the temperature dependence of the partition function and the Boltzmann relation between the total density *N* and the density $n_{v,J}$ of the level for which the absorption is measured.

Temperature measurement

The difference in temperature dependence of different absorption lines can be used to estimate the temperature of the measured species. If two absorption lines with a different temperature dependence of their line strength can be measured simultaneously, the temperature can be determined by fitting the absorption features. The temperature at which the best agreement is observed between measured and fitted signal corresponds to a first estimate of the temperature of the species of interest.

The temperature in our measurements, was determined by measuring several NO-transitions around 1870 cm^{-1}. The relative integrated absorptions of these transitions show a strong temperature dependence, which allowed for an accurate determination of the gas temperature; this turned out to be 450 K. [11]

Chapter 4

Mass Spectrometry

A mass spectrometer can be used to measure the densities of many different types of molecules simultaneously. The molecules of interest are ionized and the mass of the produced ions is determined by feeding them through a quadrupole mass filter. In this chapter the working principle of the mass spectrometer: ionization, mass selection and detection is shortly described. More details can be found in for example [12] and [13].

4.1 Introduction

Mass spectrometry is a powerful analytical technique that is used to identify unknown gas molecules and to quantify their concentrations. Compounds can be identified at very low concentrations (10^{17} m^{-3}) in chemically complex mixtures. Mass spectrometry can be used both qualitatively and, after a careful calibration procedure, also quantitatively. Because of:

- identifying molecules
- determining absolute concentrations
- low detection limits

a mass spectrometer is well suited to measure stable molecules in the background of a plasma.

4.2 Ionizer

When a molecule enters the mass spectrometer, it is ionized by an electron. The electrons are created through thermal emission from a hot filament. The filament consist of thoriated iridium and is heated up to 2000 K, resulting in thermal emission of electrons. Subsequently, the electrons are accelerated to a cage, and impact with molecules can lead to the ionization of the molecule.

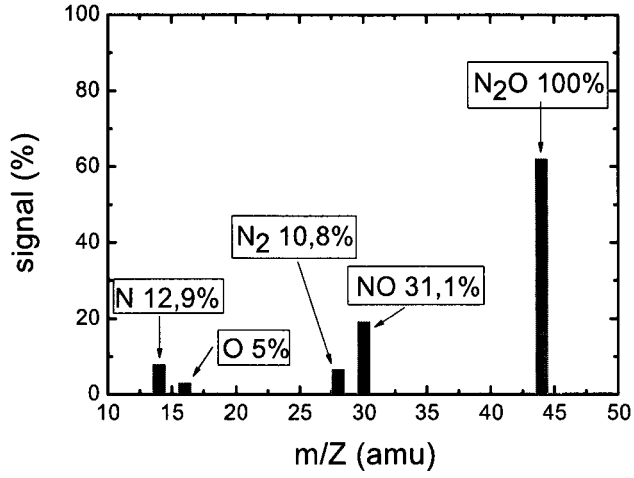

Figure 4.1: Fraction pattern for N_2O.

By varying the potential between filament and cage, the kinetic energy of the electrons can be varied. Therefore, when the energy is high enough, electrons can create double ionized molecules. Furthermore, molecules can be dissociated by electrons, producing new molecules. It is also noted that more stable isotopes exist for the same element. Therefore a molecule can be detected on different m/Z ratios. For N_2O the electron impact reactions leading to the *mass spectrum* or *fraction pattern* in figure 4.1 are [14]:

$$N_2O + e^- \rightarrow N_2 + O + e^- \tag{4.1}$$

$$N_2O + e^- \rightarrow N + NO + e^- \tag{4.2}$$

4.2.1 Mass selection

After the molecules are ionized, they are accelerated to the quadrupole mass filter. Here the mass selection occurs on their mass to charge ratio by applying electric or magnetic fields on them.

The quadrupole mass filter consists of four cylindrically shaped rods, which are electrically conducting. In figure 4.2 a cross-section of the quadrupole mass filter is given. The rods, made of molybdenum, have a diameter of 9.2 mm, a length of 200 mm and the distance between the rods is $2r = 16$ mm. A potential $\phi_0(t)$ is applied to the rods as shown in figure 4.2. This potential is given by

$$\phi_0(t) = U + V\cos(\omega t) \tag{4.3}$$

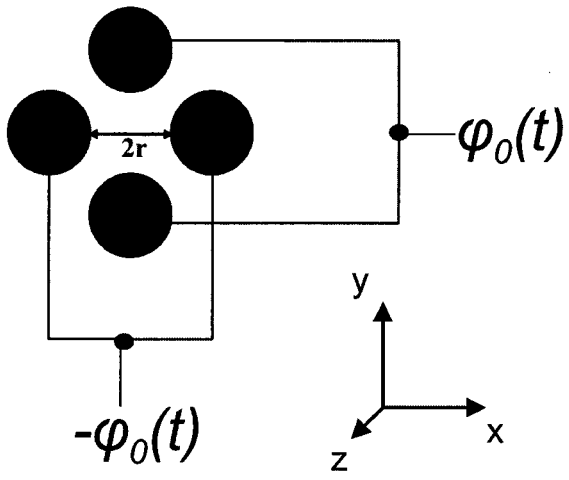

Figure 4.2: Cross section of the quadrupole mass filter.

where $\omega = 2\pi f$ with f = 2.25 MHz. The quadrupole field can then be described by

$$\phi(x,y,z) = \phi_0(t)\frac{x^2-y^2}{2r^2}. \tag{4.4}$$

The path for an ion entering the quadrupole is described by the equations of motion. Given the potential in equation 4.4, the equations in motion in the x,y and z direction are:

$$m\frac{d^2x}{dt^2} = ZeE_x = -Ze\frac{\partial\phi}{\partial x} = -\frac{Ze}{{r_0}^2}(U + V\cos(\omega t))x \tag{4.5}$$

$$m\frac{d^2y}{dt^2} = ZeE_y = -Ze\frac{\partial\phi}{\partial y} = -\frac{Ze}{{r_0}^2}(U + V\cos(\omega t))y \tag{4.6}$$

$$m\frac{d^2z}{dt^2} = ZeE_z = 0 \tag{4.7}$$

where Ze is the charge of the ion and E is the electric field. These equations are called the Mathieu differential equations. The more general form is acquired by putting:

$$u = x \ or \ y \tag{4.8}$$

$$a = \frac{4ZeU}{m\omega^2r^2} \tag{4.9}$$

$$b = \frac{2ZeV}{m\omega^2r^2} \tag{4.10}$$

$$\xi = \frac{1}{2}\omega t \tag{4.11}$$

The general form of the Mathieu equation is then:

$$\left(\frac{d^2u}{d\xi^2}\right) + (a + 2b\cos(2\xi))u = 0 \tag{4.12}$$

The solution of this differential equation is:

$$u = Ae^{\beta\xi} \sum_{n=-\infty}^{\infty} C_{2n} e^{2in\xi} + Be^{-\beta\xi} \sum_{n=-\infty}^{\infty} C_{2n} e^{-2in\xi}, \tag{4.13}$$

where A and B are parameters that depend on the starting conditions and β and C_{2n} depend on a and b.

If the solution for an ion is stable, the ion will reach the end of the quadrupole. Changing U and V makes the solution for other masses stable. By varying U linearly with V, a mass scan can be performed.

4.2.2 detector

Detection of the ions is achieved with a Faraday cup or a secondary electron multiplier.

In a Faraday cup, positive ions hit the collector, which is a steel bucket that is positioned on-axis at the end of the quadrupole mass filter. The ions are then neutralized by electrons drawn from the steel bucket. This induces a current, which is amplified and directly proportional to the number of ions and number of charges per ion.

A secondary electron multiplier (SEM) uses the principle of secondary electron emission. It consists of multiple dynodes. The first dynode emits electrons, proportional to the number of ions hitting it. These electrons are accelerated over a voltage difference of 100 V to the next dynode, creating more electrons and these are then accelerated to the next dynode and so on (17 dynodes total). In this way amplification is achieved.

The Faraday cup has a lower detection limit for the pressure in the mass spectrometer of approximately 10^{-9} Pa. The SEM however has a lower detection limit of approximately 10^{-12} Pa. Therefore, in this study the SEM is used to detect the ions. However, when using the SEM, the signals obtained from the detector, are dependent on the mass. This mass dependence is caused by the difference in ion-electron conversion efficiency for ions of different masses.

Chapter 5

Absolute calibration and accuracy of mass spectrometry measurements

5.1 Introduction

A mass spectrometer can be used to measure the densities of many different types of molecules simultaneously. The molecules of interest are ionized and the mass of the produced ions is determined by feeding them through a quadrupole mass filter. The SEM is used to detect the ions in the mass spectrometer. Detection with the SEM results in a mass dependence of the current for every molecule. Therefore, every gas has to be calibrated in order to link the ion currents to the partial pressure. In this chapter first an example of a mass scan will be given, then a calibration method will be given. Finally the procedure for analyzing data is described.

5.2 Molecules created in N_2/O_2 plasmas

In this research, plasmas produced from $Ar/N_2/O_2$ mixtures are studied. In order to find out which molecules are formed in these systems, mass scans are performed for several conditions. The m/Z channels 40 and 20 (Ar), 28 and 14 (N_2), 32 and 16 (O_2) are monitored. In order to find all other molecules which are formed, a mass scan is performed.

5.2.1 Mass scan

For different mixtures of N_2 and O_2 and different pressures, the mass scan is performed from m/Z=1 to m/Z=200. In figure 5.1 a mass scan is shown for the conditions: I_{arc}=60 A, p=13.9 Pa, 3000 sccm Ar through the arc, 880 sccm N_2 + 1100 sccm O_2 into the background. The peaks are indicated

Table 5.1: m/Z values for the corresponding molecules at their maximum signal

Molecule	m/Z
Ar	40
N_2	28
NO	30
O_2	32
N_2O	44
NO_2	46
H_2O	18
H_2	2

with the corresponding molecule. Besides Ar, N_2 and O_2, also NO, N_2O and NO_2 were detected. In table 5.1 the values for the m/Z are given at which the maximum signals are detected for each molecule.

In figure 5.1 other molecules than N and O containing molecules are detected, which can not be formed from the injected gases. For example H_2O is observed at m/Z=18 and H_2 is observed at m/Z=2.

Note that in this mass scan also isotopes can be seen, like ^{36}Ar (0.33%), ^{38}Ar (0.06%) and ^{15}N (0.37%). The percentages indicate the relative signal compared to the maximum signal of the corresponding molecule.

5.2.2 Discussion

In the mass spectrometer there is always a background pressure of the order of magnitude 10^{-9} mbar. A typical measurement is performed at $4 \cdot 10^{-7}$ mbar or $2 \cdot 10^{-6}$ mbar. The background is caused from an in leak of air and we will always observe signals for H_2O, N_2, O_2 and CO_2. However, during the measurement, the densities of these molecules are small compared to those from molecules added to or generated in the plasma. Furthermore they are approximately constant during a measurement. When the plasma is on, the temperature in the vessel rises and more H_2O desorbs from the walls of the reactor or the mass spectrometer. The mass spectrometer is attached downstream to the setup and the temperature changes in the reactor will not affect the temperature in the mass spectrometer. Therefore, the rise in the signals for H_2 and H_2O can most likely be ascribed to a higher desorption rate in the vessel due to a higher temperature in the vessel.

The CO_2 fraction causes a signal at m/Z=44. At m/Z=44 N_2O has also its largest signal. The signal at m/Z=44 can be corrected for CO_2 signal from the background. However when the O_2 flow is increased, the signal on m/Z=44 seems also to increase. It is possible that the O_2 gas feed lines have a small CO_2 contamination. Due to the fraction pattern for CO_2, 10% of the CO_2 signal on m/Z=44 is measured at m/Z=28 (CO^+), where also

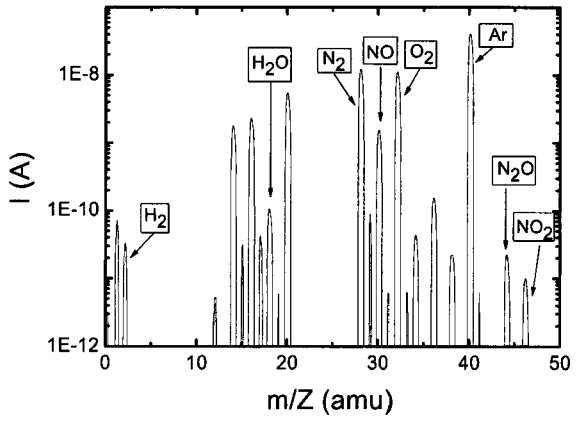

Figure 5.1: Mass scan for an Ar plasma with N_2 and O_2 injected in the vessel. The plasma conditions are: I_{arc}=60 A, p=13.9 Pa, 3000 sccm Ar through the Arc, 880 sccm N_2 + 1100 sccm O_2 into the vessel. The peaks are indicated with the corresponding molecule. Besides Ar, N_2 and O_2, also NO, N_2O and NO_2 were detected.

N_2 is measured. But this fraction is in the order of the background signal of N_2 and thus it can be ignored for the signal at m/Z=28.

5.3 Calibration

In this section the calibration procedure is presented. At the end of the section a measurements is shown in which the concentration determined with calibrations factors obtained from the calibration procedure, is compared with concentration determined with TDLAS.

In the interpretation of mass spectra, the following assumptions are made [16]):

- Each molecule gives a constant mass spectrum, characteristic of the molecule.
- The spectrum of a mixture is the same as that obtained by the linear superposition of individual spectra of the gases in the mixture.
- The ion current, which corresponds to a particular peak is proportional to the partial pressure of the gas in the mix responsible for that peak.

The following relation should be found for the ion current and the partial pressure of the corresponding molecule:

$$I(X) = CF(X)p(X) \tag{5.1}$$

where I is the ion current for a molecule, p(X) is the partial pressure of molecule X in the vessel and CF is the relation between the ion current and the partial pressure.

To operate in a large pressure range in the process chamber, the calibration is performed on the partial pressure in the mass spectrometer. While the pressure in the vessel can be varied, the pressure in the mass spectrometry can be kept at its optimal operating pressure through regulating the valve (see figures 3.1 and 3.2). The calibration factor used in this study can be expressed as:

$$CF(X) = \frac{I(X)}{p_{MS}(X)} \tag{5.2}$$

Because from the partial pressures in the mass spectrometer, the molar fraction can be determined, which is assumed to be equal to the molar fraction in the process chamber. From the molar fraction the partial pressures in the vessel can be determined. However, it is assumed that the molar fraction in the vessel is equal to the molar fraction in the mass spectrometer. For this assumption we have to consider the valve, between the mass spectrometer and the vessel, and the pumping speed of the turbopump S.

In our setup a valve is attached between the mass spectrometer and the plasma vessel (see figures 3.1 and 3.2). Therefore the relation between the partial pressure of a particle in the plasma vessel and the partial pressure of a particle in the mass spectrometry are described by:

$$p_{MS}(X) = p_{vessel}(X)\frac{C(X)}{S(X)} \tag{5.3}$$

Where C is the conductance of the valve and S is the effective pumping speed of the turbopump. The flow in the valve is in the molecular regime. Therefore, the conductance of the pinhole can be written as

$$C = \frac{1}{4}\sqrt{\frac{8kT}{\pi m}}A \tag{5.4}$$

where A is the area of the aperture of the valve and m is the mass of the molecule. The mass dependence in equation 5.1 cancels out, because C has a $1/\sqrt{m}$ dependence and S has also $1/\sqrt{m}$ dependence, because heavier particles have a lower average speed after the valve (for equal temperature). Hence the ratios between the partial pressures in the plasma vessel remain equal to the ratios of the partial pressures in the mass spectrometer. In other words, the fraction of the molecules in the mass spectrometer and the vessel are equal.

Calibrating gases is performed in two ways.

1. Calibrating common gases in stock by regulating valve aperture: *direct calibration*

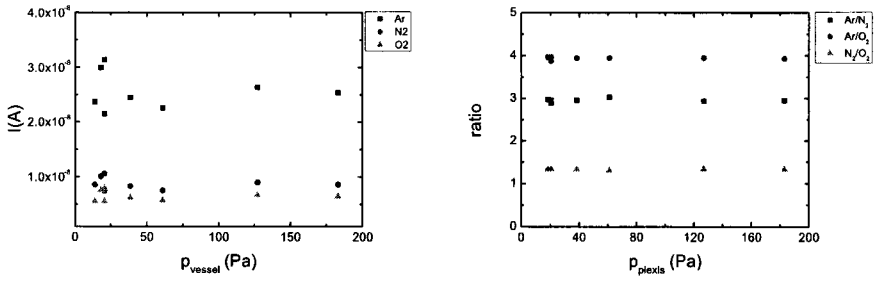

(a) current (b) current ratio

Figure 5.2: In a) the ion currents are plotted as a function of the pressure. In b) the ratio of the ratio between the ion currents are plotted, hence it is noted that the ratios remain constant.

2. Calibrating gases not in stock with the help of another diagnostic tool (TDLAS): *indirect calibration*

Common gases like Ar, N_2 and O_2 can be directly calibrated. A constant flow for one single gas is let in the vessel. The vessel is kept at a constant pressure. The pressure in the mass spectrometry is now varied with the valve and with equation 5.2 the calibration factor can be determined.

Gases which are not in stock, like N_2O have to be calibrated otherwise. By measuring the concentration with TDLAS, the partial pressure can be determined. By measuring simultaneously the ion current with the mass spectrometer, the calibration factor for N_2O can be determined with equation 5.2.

The calibration factors have to be normalized on Ar, because the sensitivity of the mass spectrometer changes in time. To show that the relative sensitivity change for all molecules is equal, the following measurement is performed. Flows of Ar, N_2 and O_2 are fed to the vessel in a way that the molar fractions for Ar, N_2 and O_2 are respectively 0.62, 0.19 and 0.19. The pressure in the vessel is varied ranging from 10 to 200 Pa. The pressure of the mass spectrometry is kept constant at $4{\cdot}10^{-7}$ mbar. The ion currents are now plotted against the pressure in the vessel. From figure 5.2a) it can be seen that while the molar fractions in the vessel remain constant, the ion currents do not. But from 5.2b) it can be seen that the ratio of the currents does remain constant. The same measurement is now plotted against time in figure 5.3. It seems that the sensitivity of the mass spectrometer changes in time for all molecules, however the ratio remains constant. The relative change in the sensitivity of the mass spectrometry for a molecule is equal for all molecules. Therefore normalization on Ar is justified. Therefore every calibration factor is normalized to the Ar calibration factor. The calibration

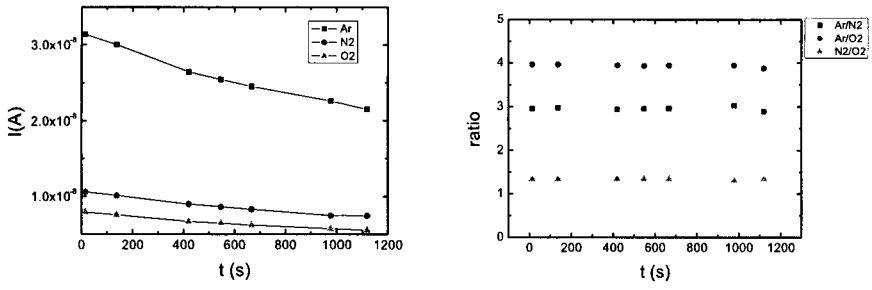

(a) current (b) relative current

Figure 5.3: In a) the molar fractions are plotted. In b) the ratio of the molar fractions are plotted, hence it is noted that the ratios remain constant.

Table 5.2: Normalized calibration factors on Ar.

Gas	Ar	N_2	O_2	NO	N_2O	NO_2	H_2O	NH_3	H_2
CF_{norm} (A/mbar)	1	0.98	0.75	1.4	0.7	0.7	0.87	1.02	1.6

factor of Ar on which it is normalized, is determined right before or after the calibration of the specific molecule.

$$CF_{norm}(X) = \frac{CF(X)}{CF(Ar)} \tag{5.5}$$

In figure 5.4 an example is given of an Ar calibration. The assumption that the partial is pressure is linearly dependent on the current is clearly seen. This behavior is found for all calibrations.

In table 5.2 normalized calibration factors for several molecules are given.

A measurement on a plasma is shown in figure 5.5 in which the partial pressure of NH_3 is determined with mass spectrometry and from TDLAS measurements. The plasma conditions are: 3000 sccm Ar through the arc, I_{arc}=70 A, p=20 Pa and an NH_3 flow increasing from 0 to 1438 sccm. The calibration factor used for measuring the molar fractions measured with mass spectrometry, are directly calibrated. Hence, the molar fractions acquired with TDLAS and mass spectrometry are independent. As can be seen from the figure, the results show good agreement with each other.

Finally a measurement is shown in figure 5.6 in which the molar fractions in the vessel are compared with the molar fractions in the mass spectrometer. The conditions are identical to the conditions of the measurements discussing the sensitivity of the mass spectrometer for all molecules. The molar fractions in the vessel, calculated from the injected flows, show good agreement with the molar fractions in the mass spectrometer, calculated with the cal-

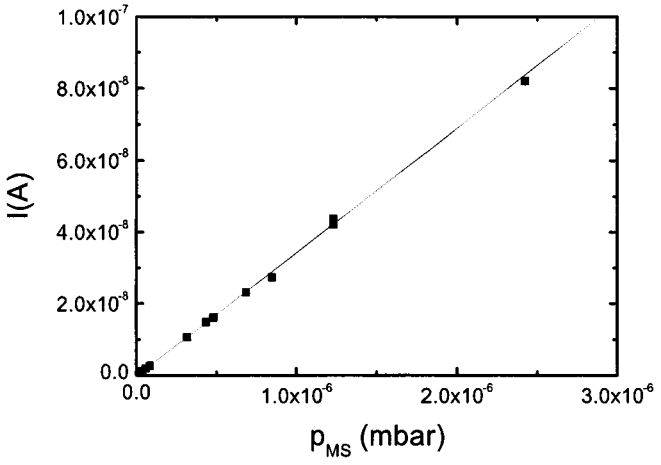

Figure 5.4: Signal of Ar measured for different pressures in the mass spectrometer during a calibration.

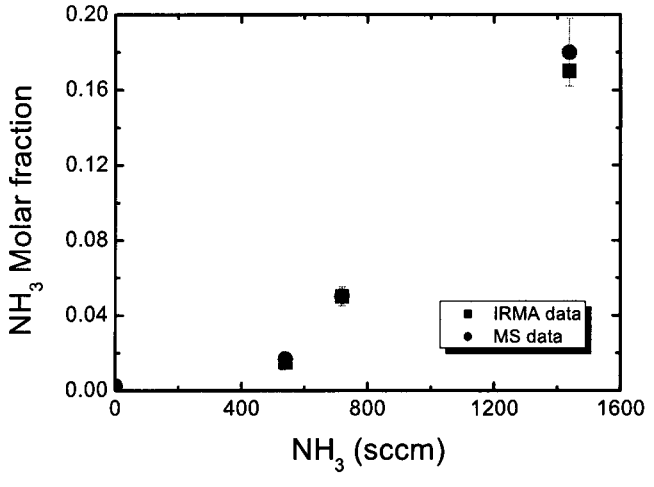

Figure 5.5: NH_3 molar fraction in an Ar/NH_3 plasma determined independently by TDLAS and mass spectrometry.

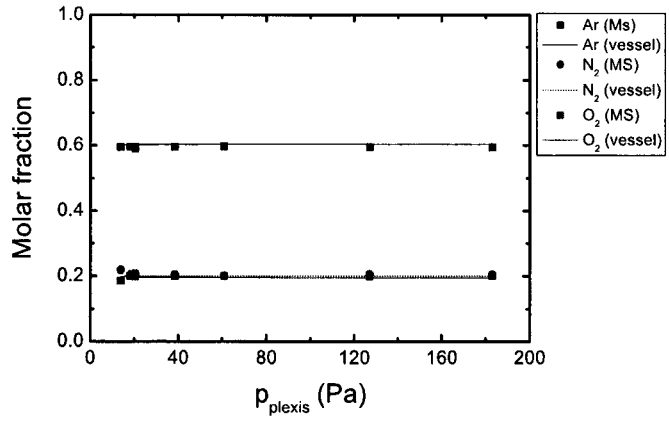

Figure 5.6: The molar fractions in the vessel, calculated from the injected flows, show good agreement with the molar fractions in the mass spectrometer, calculated with the calibration factor.

ibration factor.

5.4 Procedure for analyzing data

In this section, a procedure will be shown, to analyse the raw data obtained from mass spectrometry measurements. Finally a method will be given in which the accuracy of the measurement can be checked. During the explanation of the procedure for analyzing rough data obtained from mass spectrometry, an example of a measurement will be given on which this procedure is applied.

Rough data

A measurement is taken in which O_2 and N_2 are admixed to an Ar arc. The plasma conditions are: 3000 sccm through the arc, I_{arc}=75 A, 1900 sccm N_2 + O_2 in the background.

First the raw data is plotted in figure 5.7: the currents are plotted versus the time. From this plot the conditions can be filtered by selecting the stable signal corresponding to the particular condition and worked out before being analyzed.

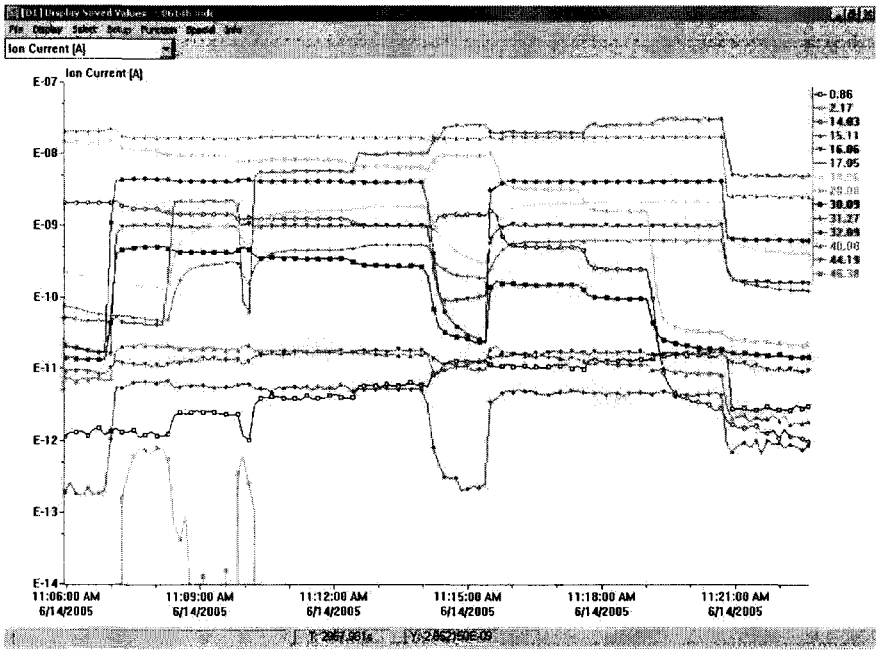

Figure 5.7: Representation of all the signals corresponding to the m/Z numbers. On the x-axis the absolute time is given.

correcting for background signals

For every mass over charge (m/Z) current, the background signal has to be subtracted. The background for every signal is determined by taking its value during a condition where only the Ar plasma is burning and no other gases are injected. These background values are subtracted from their corresponding *m/Z* signals.

calculating the fraction

Every signal is then multiplied with its corresponding *normalized calibration factor*. The molar fraction of for example NO is obtained as follows. The signal for NO is multiplied with its normalized calibration factor. This is divided by the sum of every signal multiplied with its corresponding *normalized calibration factor*. In formula form this is:

$$NOfraction = \frac{\big(I(NO) - I_{bg}(NO)\big) \cdot C_{norm}(NO)}{\sum_n \big(I(n) - I_{bg}(n)\big) \cdot C_{norm}(n)} \tag{5.6}$$

In the formula *I(NO)* is the current measured at m/Z=30. I_{bg}*(NO)* is the background current for m/Z=30 at a condition where no NO can be formed. C_{norm}*(NO)* is the normalized calibration factor voor NO, n is the integer to denote every molecule.

normalization factor

Now a procedure will be shown to obtain the partial pressures in the mass spectrometer and how to compare these to the pressure measured with the ionization gauge.

First the calibration factor for Ar is determined, with a condition in which only Ar is used. Ar is calibrated by dividing the current of the signal at m/Z=40 by the real pressure in the mass spectrometer. The real pressure in the mass spectrometer is obtained by dividing the measured pressure on the IMG ionization gauge with the *relative sensitivity R*. The *relative sensitivities* [15] are given in chapter 3.

The pressure meter we use to measure the pressure in the mass spectrometer is an ionization gauge. This ionization gauge is calibrated for nitrogen and the relative sensitivity for N_2 is then 1. But for example Ar the relative sensitivity is larger, namely 1.3. This means that for the same pressure the ionization gauge indicates a pressure that is 1.3 times higher than the real pressure.

Therefore when calibrating Ar by dividing the current with the pressure in the mass spectrometer in a condition where there is only Ar present in the mass spectrometer, the pressure obtained from the ionization gauge has to be divided by R_{Ar}=1.3:

$$C(Ar) = \frac{I(Ar) - I_{bg}(Ar)}{p_{IMG}/R_{Ar}} \tag{5.7}$$

p_{IMG} is the pressure in the mass spectrometer measured with the ionization gauge, R_{Ar} is the relative sensitivity for Ar. The absolute calibration factor for Ar is then multiplied with the normalized calibration factors to obtain the absolute calibration factors for all molecules. The background corrected signals are then multiplied by the absolute calibration factors to obtain the the partial pressures in the mass spectrometer:

$$p_{part}(X) = C_{norm}(X) \cdot C(Ar) \cdot \big(I(X) - I_{bg}(X)\big) \tag{5.8}$$

$p_{part}(X)$ is the partial pressure in the mass spectrometer for molecule X, C(Ar) is the absolute calibration factor for Ar, $C_{norm}(X)$=the normalized calibration factor for molecule X. When all these partial pressures are multiplied with its corresponding *relative ionization sensitivity R* and added up, the measured pressure is obtained:

$$p_{IMG} = \sum_n \frac{C_{norm}(n) \cdot C(Ar)}{R_n} \cdot \big(I(Ar) - I_{bg}(Ar)\big) = \sum_n \frac{p_{part}(n)}{R_n} \tag{5.9}$$

p_{IMG} is the pressure measured with the ionization gauge, n is the integer to denote every molecule.

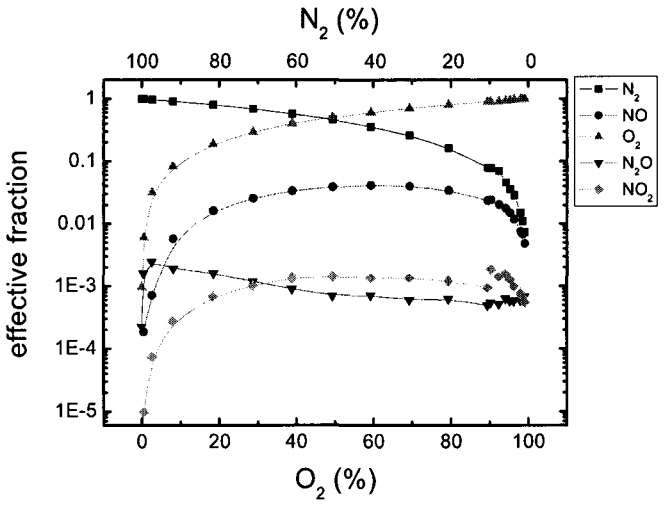

Figure 5.8: The effective fractions are plotted versus the ratio between the injected gases.

Result

In figure 5.8 the results obtained with this procedure is plotted for a measurement in which the injected N_2 and O_2 flows in the background of an Ar arc, are varied. In the figure fractions down to 10^{-5} are measured. This corresponds to partial pressures of $\sim 10^{-10}$ Pa in the mass spectrometer and $\sim 10^{-4}$ Pa in the process chamber, which means that species with partial pressures down to $\sim 10^{-4}$ in the process chamber can be detected.

5.5 Accuracy check of measurements

5.5.1 Introduction

In the calibration chapter the accuracies of the calibration factors were discussed. In this section a method is introduced to check the accuracy of a typical measurement.

An accuracy check is performed by comparing *filling* fractions and *measured* fractions. *Filling* fraction for N atoms and O atoms are values we obtain from the injected flows. As an example, for an injected flow of 70 sccm N_2 and 30 sccm O_2 we obtain a filling fraction value of 0.7 for N and 0.3 for O. *Measured* fraction for N and O atoms are entirely obtained from measured data. For determining the filling fraction, well calibrated flow meters and pressure meters are used.

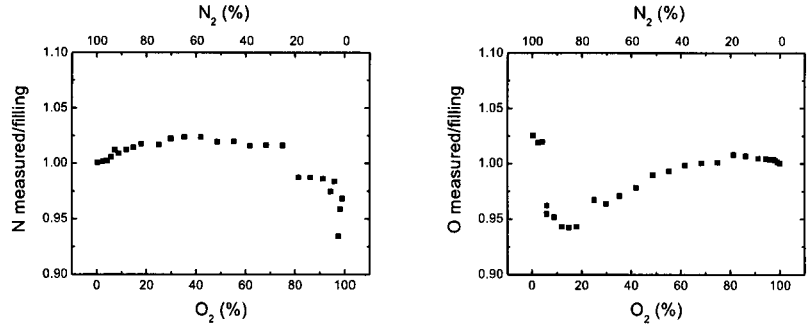

(a) N(measured)/N(filling) (b) O(measured)/O(filling)

Figure 5.9: The ratio between *measured* values and *filling* values are plotted to check the accuracy of the measurment. The plasma conditions for this measurement are: I_{arc}=75 A, p=20 Pa, 5000 sccm Ar through the Arc, 900 sccm N_2 + O_2 into the background.

5.5.2 Results and discussion

This method is applied on a typical measurement to check the accuracy. In figure 5.9 the ratio of the measured fraction and filling filling is plotted versus the fraction of the injected gases. For these measurements, the *filling* and *measured* fraction of N and O atoms can be described as:

$$N_{\text{filling}} = \frac{2\phi(N_2)}{2\phi(N_2) + 2\phi(O_2)} \tag{5.10}$$

$$O_{\text{filling}} = \frac{2\phi(O_2)}{2\phi(N_2) + 2\phi(O_2)} \tag{5.11}$$

$$N_{\text{measured}} = \frac{\#N}{\#N + \#O} \tag{5.12}$$

$$O_{\text{measured}} = \frac{\#O}{\#N + \#O} \tag{5.13}$$

Here ϕ is the flow and #N and #O the total amount of N respectively O particles, as measured in all molecules detected by the mass spectrometer. From the figure we can observe that for the whole range of the ratio of the injected O_2 and N_2 the accuracy is within 5% for both N and O.

Figure 5.9a) shows a minimum in the ratio of the measured over filling values for N, when low fractions of N_2 are admixed. The same is seen for the ratio of the measured and filling values for O, when low fractions of O_2 are admixed in figure 5.9b). Possible explanations are given below for these observations.

At low fractions of the admixed O_2 or N_2 the other molecules like NO, N_2O and NO_2 become more dominant. (In measurements in the next sections this will be shown.) Uncertainties in the calibration factors of those

molecules are larger than those for N_2 and O_2. Because of this, the error in the total measured N or O becomes larger. Then in the regime with low fractions of the admixed O_2 we would expect the largest deviation for the ratio of measured and filling for O and in the regime with low fractions of the admixed N_2 regime we would expect the largest discrepancy for the N measured over filling. This is indeed what we observe.

The calibration for the mass flow controllers for very low ($< 2\%$ of maximum flow) flows introduces also an error. However, in the most extreme case, which is at 0.5 O_2 % flow, we make an error of 6 % with the calibration compared to the measured value for that condition.

The accuracy check shows that for the whole regime the measurement shows good accuracy.

5.6 Conclusions

In this section a mass scan is shown for an $Ar/N_2/O_2$ plasma. A calibration method is introduced and a procedure for analyzing the data is given. Also the fraction of the molecules in the process chamber are compared with the fractions in the mass spectrometer for several conditions. Furthermore, the sensitivity of the mass spectrometer has been investigated for several conditions. The concentrations measured simultaneously with mass spectrometry and TDLAS, have been compared and fractions. Finally a method is shown to check the accuracy of a measurement.

Mass scans showed that in an N_2/O_2 plasma besides Ar, N_2 and O_2, also NO, N_2O and NO_2 are detected. Fractions of the molecules in the process chamber are always equal to the fractions in the process chamber. Therefore the valve can be used at different openings. Hence always the optimum pressure in the mass spectrometer can be regulated and calibrations can be performed by regulating the valve, which is the main advantage over using a pinhole.

The relative sensitivity change in the mass spectrometer spectrometer for the molecules is equal for all molecules. Therefore calibrations are normalized on Ar.

The concentrations determined with mass spectrometry show agreement within 10% with concentrations determined with TDLAS.

By using the valve instead of a pinhole, always the maximum signal(s) can be obtained for different pressures in the process chamber. Because when using a pinhole, the signal(s) in the mass spectrometer could become smaller than the detection limit at very low pressures in the process chamber or the pressure in the mass spectrometer could exceed the maximum operating pressures of the mass spectrometer for high pressures in the proces chamber. Therefore, when using a pinhole, the pressure range is limited in the process chamber at which the mass spectrometer can be used. This range is much

larger when using a valve, because always the optimum pressure in the mass spectrometer can be used.

Finally, the accuracy check shows that for the whole regime the measurement shows good accuracy.

Chapter 6

N_2/O_2 plasmas

6.1 Introduction

As described in 1, plasmas containing N_2 and O_2 are widely used to treat surfaces, for example for etching of photoresist material. But this type of plasma is also encountered in the shuttle glow phenomenon: a plasma formed at the nose of the space shuttle during re-entry in the earth atmosphere. Unfortunately, detailed knowledge on the processes taking place during the interaction between a plasma containing N_2 and O_2 and a surface is lacking.

Brussaard et al. [17] investigated the photoresist etch rates with an Ar/O_2 and $Ar/O_2/N_2$ plasma. They observed higher etch rates when nitrogen was admixed even for only small fractions of admixed N_2. The increase in etch rate when nitrogen is added is explained by the fact that nitrogen atoms react with oxygen molecules in the downstream plasma to form nitric oxide and additional oxygen atoms.

$$N + O_2 \rightarrow NO + O \tag{6.1}$$

The so-called shuttle glow phenomenon is a second example where N_2/O_2 plasmas are encountered. During the re-entry of a space shuttle in the earth atmosphere, an orange glow is observed under the space shuttle. This is most likely the effect of large fluxes of radicals impinging on the surfaces of the spacecraft [18] [19]. A similar effect is observed in an expanding thermal plasma created from a mixture of N_2 and O_2, when a high flux of radicals interact with a (copper) surface. This is shown in figure 6.1.

In both of these examples, a high flux of radicals is directed onto a surface. In this chapter an extensive set of measurements on N_2/O_2 containing plasmas is presented and the processes taking place in the gas phase and at the surfaces are investigated.

First, in section 6.2 the surface and surface interactions in N_2 and O_2 plasmas are discussed. In section 6.3 the molecular abundances in plasmas containing a varying fraction of N_2 and O_2 are investigated. By means

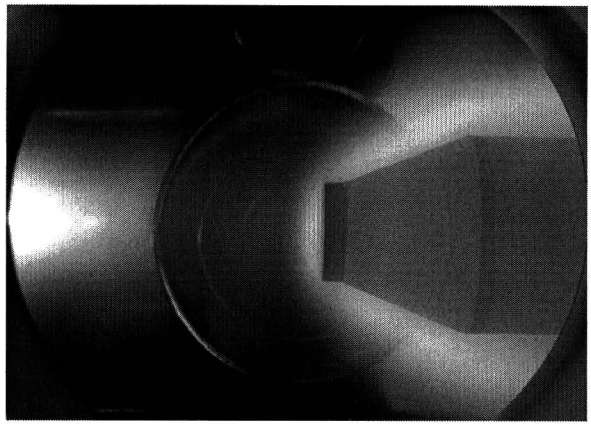

Figure 6.1: Interaction between a high flux of plasma produced N and O radicals and a copper surface, leading to electronically excited molecules (NO_2) which cause the orange glow.

of pressure dependence measurements presented in section 6.5, the relative importance of reactions in the gas phase and reactions at the surfaces for the final gas composition, is investigated. In section 6.6 the measured conversion of N_2 and O_2 into N_2O is compared with the maximum possible conversion. Finally in section 6.7 a comparison of the data from measurements with different conditions is given.

6.2 Surface coverage

In this section the surface coverage is discussed together with surface reactions.

If we assume that all radicals created in the plasma will arrive at the surface, which is shown to be reasonable in chapter 2, the surface coverage will at least partly be determined by the amount of radicals created. Next to the amount of radicals, also the sticking probability of the radicals on stainless steel, will determine the surface coverage. Singh et. al. have determined the sticking probabilities of N_2 and O_2 in pure N_2 and O_2 plasmas respectively. The sticking probability for N and O are respectively 0.07 ± 0.02 and 0.17 ± 0.02 [20]. If only the sticking probability is considered, then we would expect for a injected ratio of N_2 and O_2 of one, a higher O coverage than N coverage. Furthermore, measurements performed by Van Helden et. al. [11], in which Ar plasmas with mixtures of N_2 and O_2 in the background were studied, showed that N and NO diffuse into the wall.

Now a model for the surface coverage, dependent on the ratio of the injected N_2 and O_2, will be given which was proposed by Van Helden et. al. [11]. Radicals or atoms and molecules at the surface will be indicated with the subscript s in the reactions. Radicals or molecules in the wall will be

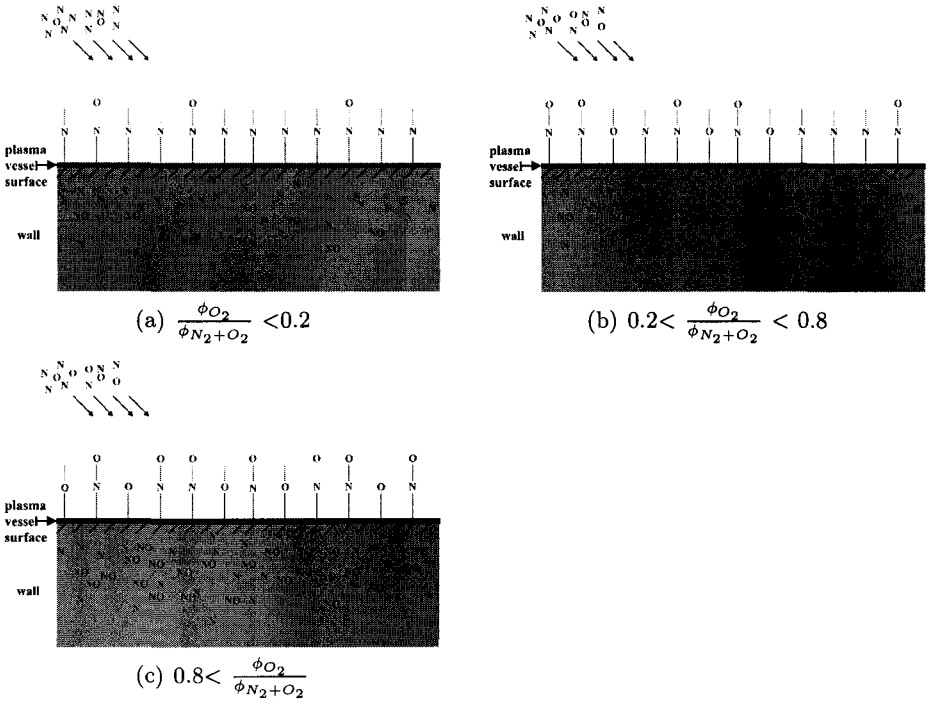

(a) $\frac{\phi_{O_2}}{\phi_{N_2+O_2}}$ <0.2 (b) 0.2< $\frac{\phi_{O_2}}{\phi_{N_2+O_2}}$ < 0.8

(c) 0.8< $\frac{\phi_{O_2}}{\phi_{N_2+O_2}}$

Figure 6.2: For three flow regions, the surface coverage is depicted.

denoted with the subscript w.

- For ratios of $\frac{\phi_{O_2}}{\phi_{N_2+O_2}}$ <0.2, the surface is covered with mainly N atoms and NO molecules. Mainly N atoms are stored in the wall. NO can be formed through association of N and O at the surface. In figure 6.2a) this situation is schematically shown.

- For ratios of $\frac{\phi_{O_2}}{\phi_{N_2+O_2}}$ between $\sim$ 0.2 and $\sim$ 0.8, the surface is covered with N and NO particles and with O atoms. In the wall again N and NO are stored with higher fractions of NO, as shown in figure 6.2b).

- For ratios of $\frac{\phi_{O_2}}{\phi_{N_2+O_2}}$ > $\sim$ 0.8, the surface is covered with O and NO. O atoms will be the most abundant. Any N_s at the surface will most likely associate with an O atom to form NO_s. In figure 6.2c) this is illustrated.

If now the incoming N and O radicals are considered together with the

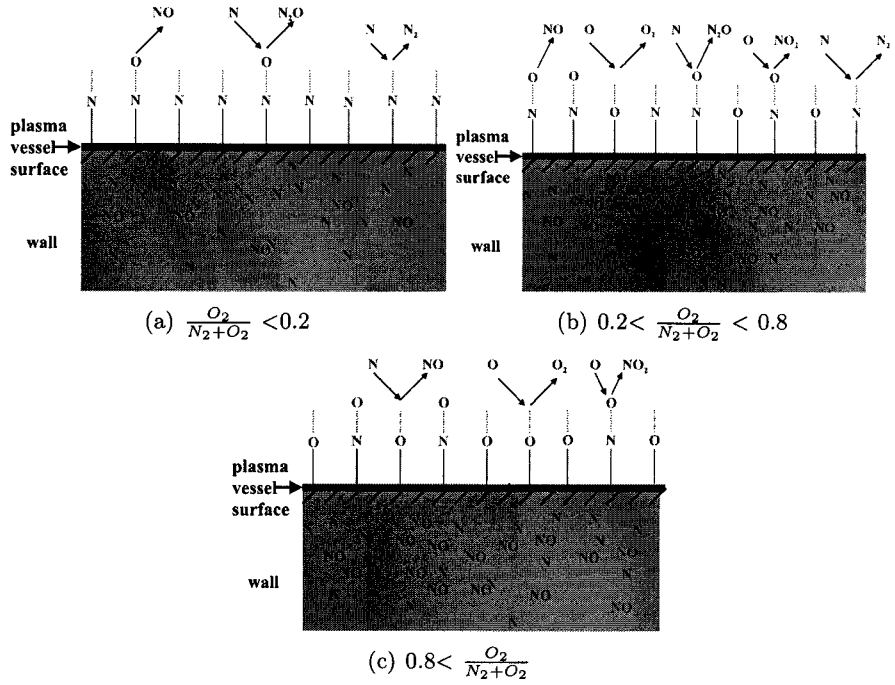

(a) $\frac{O_2}{N_2+O_2}$ <0.2 (b) 0.2< $\frac{O_2}{N_2+O_2}$ < 0.8

(c) 0.8< $\frac{O_2}{N_2+O_2}$

Figure 6.3: Surface reactions. For al three regions the most important surface reactions are depicted.

surface coverage, then theoretically the most likely surface reactions are:

$$N + NO_s \rightarrow N_2O \quad (6.2)$$
$$O + NO_s \rightarrow NO_2 \quad (6.3)$$
$$N + N_s \rightarrow N_2 \quad (6.4)$$
$$O + N_s \rightarrow NO_s \quad (6.5)$$
$$NO_s \rightarrow NO \quad (6.6)$$
$$O + O_s \rightarrow O_2 \quad (6.7)$$
$$N + O_s \rightarrow NO_s \quad (6.8)$$

In figure 6.3 a schematic representation is given of these surface reactions. For each region the most important reactions are given. In the results the data are discussed in terms of *molar fraction*, *effective fraction* or *atomic fraction*. The molar fraction is the partial pressure of a molecule divided by the total pressure. But because Ar is an inert gas it does not interact in the formation or dissociation of molecules and molecules containing Ar will not be formed. Ar^+ ions only dissociate N_2 and O_2 molecules. That is why the effective fractions are used to plot and discuss our data. The effective fraction is the partial pressure of a molecule divided by the total pressure from which the partial pressure of Ar is subtracted. The atomic fraction of

a particular atom Y in a particular molecule X is determined by dividing the amount of atoms Y in that molecule X by all atoms Y in the system. In formula from the molar fraction, the effective fraction and the atomic fraction are then:

$$\text{molar fraction (X)} = \frac{p_{\text{part}}(X)}{p_{\text{total}}} \tag{6.9}$$

$$\text{effective fraction (X)} = \frac{p_{\text{part}}(X)}{p_{\text{total}} - p_{\text{part}}(Ar)} \tag{6.10}$$

$$\text{atomic fraction (Y)in(X)} = \frac{a_Y(X) \cdot p_{\text{part}}(X)}{\sum_n a_Y(n) \cdot p_{\text{part}}(n)} \tag{6.11}$$

In the formule is X a molecule, p_{part}(X) is the partial pressure of molecule X, p_{total} the total pressure, Y is an atom, a_Y(X) is a integer expressing the number of an Y atom in one molecule X.

6.3 Plasmas created from mixtures of N_2 and O_2.

From the N and O radicals produced in the plasma expansion, new molecules can be formed, in the gas phase or at the surface of the reactor. By studying different mixtures of N_2 and O_2, in which the ratio between these two gases is varied and therefore the ratio between the N and O radicals, the importance of the gas phase and surface reactions are investigated together with the surface coverage. These measurements will be called *mixture measurements.*

The sum of the injected N_2 and O_2 flows is kept constant during one measurement serie. The Ar flow through the arc and the arc current I_{arc} are also kept constant. The amount of Ar^+ ions remains constant, as described in section 6.2 and in the section describing the ETP. Thus also the total amount of radicals remains constant, but the ratio of N and O atoms changes with changing ratio of the injected N_2 and O_2 flows.

To investigate the pressure dependence, the mixture measurements will be performed at 9, 20 and 100 Pa. Mixture measurements at pressures down to 5 Pa have been performed with an Ar/He arc, but these are not completely understood. They are given in appendix B.

6.3.1 Results

The mixture measurements are performed at 9, 20 and 100 Pa. For the mixture measurement at 20 and 100 Pa the plasma conditions are: I_{arc}=75 A, 3000 sccm Ar through the Arc and 1900 sccm N_2 + O_2 into the background. For the mixture measurement at 9 Pa the plasma conditions are: I_{arc}=75 A, p=9 Pa, 1525 sccm Ar through the Arc and 900 sccm N_2 + O_2 into the background. At 9 Pa we choose lower flows in order to achieve this low pressure.

In figure 6.4 the effective fractions of all molecules are plotted versus the fraction of admixed O_2. From left to right the fraction of the admixed O_2 increases and the fraction of the admixed N_2 decreases. In a) the mixture measurement at 9 Pa, in b) at 20 Pa and in c) at 100 Pa are plotted. From figures 6.4a) to 6.4c) it is observed that NO is the most abundant molecule besides N_2, O_2 and argon. For all three pressures, NO has its maximum effective fraction at a fraction of 60% of the admixed O_2 (or at a fraction of 40% of the admixed N_2.) NO_2 was already observed from the mass scan performed at a pressure of 13.9 Pa in section 5.2. At 100 Pa (see figure 6.4c)however, hardly any NO_2 is seen. Furthermore it is observed from figures 6.4 a) and b) that the trend of the NO_2 effective fraction is identical to the trend of the NO effective fraction. The N_2O effective fractions show a maximum at low admixed O_2 fraction.

We will first focus on the trends of the NO effective fraction at different pressures. In figure 6.5 the NO effective fraction is plotted, from the mixture measurement at 20 Pa in figure 6.4 b). We can see in this figure and from the enlarged plot in the inset, that at fractions lower than 4% of the admixed O_2 hardly any NO is observed. However, going to larger fractions of the admixed O_2, the NO fraction shows a fast increase. This behavior that we observe in the regime for low fractions of the admixed O_2 (up to a fraction of 4 % of the admixed O_2 in this measurement) we will call from now on *threshold behavior* or just *threshold*. This threshold behavior can also be seen in the paper by Gordiets et al [21], however it is not discussed in that paper.

In figure 6.6 the NO effective fraction is plotted for all three pressures to see whether this threshold behavior is also observed at other pressures. From this figure and the enlarged plot in the inset, we observe this threshold for the mixture measurements at 20 Pa and at 100 Pa. But for the mixture measurement at 9 Pa there is no threshold observed. It seems that the threshold becomes smaller for lower pressures. In figure 6.6 we can also see that the maximum of the NO fraction remains at a fraction of 60 % of the admixed O_2 for all pressures. But with increasing pressure, the maximum value of the NO fraction increases.

In order to examine in detail the N_2O behavior, the N_2O effective fractions for all three pressures are plotted versus the fraction of the admixed O_2 in figure 6.8. At 9 Pa, the lowest pressure, the highest peak for the N_2O fraction is observed. For increasing pressure, the maximum value of the peak decreases. For higher fractions of the admixed O_2 (higher than 5%), the decrease in the N_2O fraction with increasing pressure is much more clear. However, the increase in the N_2O fraction with increasing fraction of the admixed O_2 at low fractions of the admixed O_2 is identical. The only difference is that the increase stops slightly earlier with increasing fraction of the admixed O_2 for increasing pressure. Furthermore, figure 6.4 shows that the N_2O fraction has a maximum value around a fraction of 4 % of the

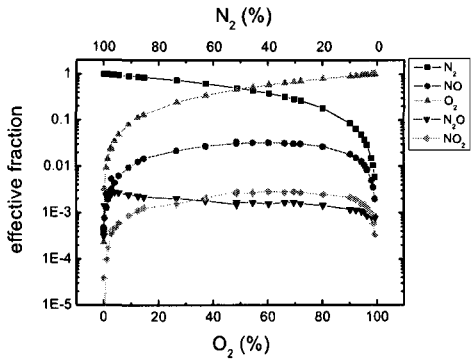

(a) p=9Pa

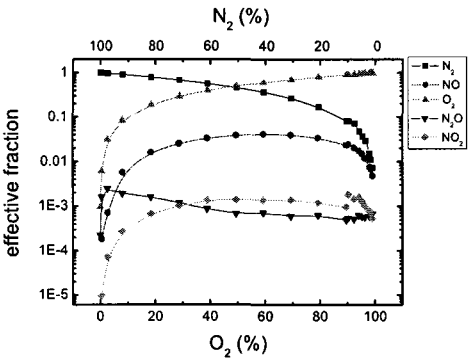

(b) p=20Pa

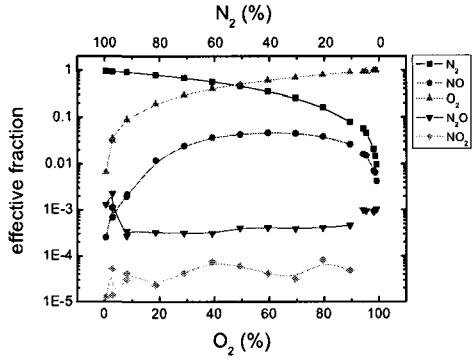

(c) p=100Pa

Figure 6.4: In the figures the fractions of the molecules are plotted versus the ratio of the injected O_2 and N_2. On the bottom x-axis the fraction of the admixed O_2 is plotted and at the top x-axis the fraction of the admixed N_2 is plotted. For the mixture measurement at 9 Pa the plasma conditions are: I_{arc}=75 A, 1525 sccm Ar through the Arc, 900 sccm N_2 + O_2 into the background. For the mixture measurements at 20 and 100 Pa the plasma conditions are: I_{arc}=75 A, 3000 sccm Ar through the Arc, 1900 sccm N_2 + O_2 into the background.

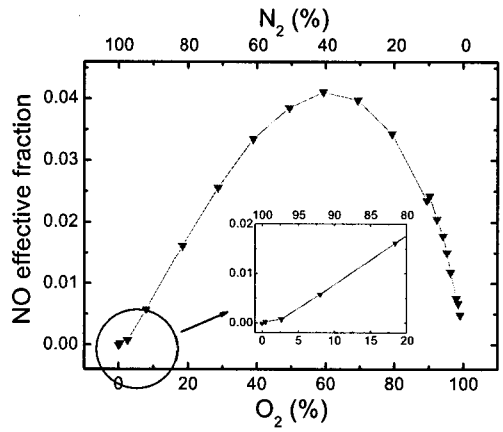

Figure 6.5: The effective NO fraction is plotted for the N_2 and O_2 mixture measurements at 20 Pa. In the figure the regime for low fractions of the admixed O_2 is blown up to clearly display the threshold behavior.

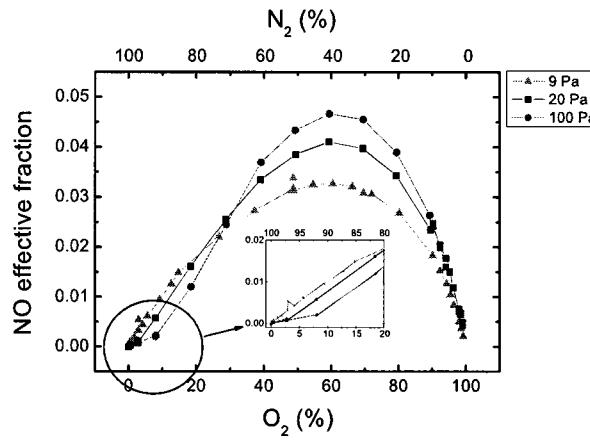

Figure 6.6: The effective fractions of NO from the N_2 and O_2 mixture measurements at 9, 20 and 100 Pa are plotted to determine possible pressure dependencies for the NO fraction. From the enlarged plot in the insert it is seen that the threshold behavior increases with increasing pressure together with the maximum of NO.

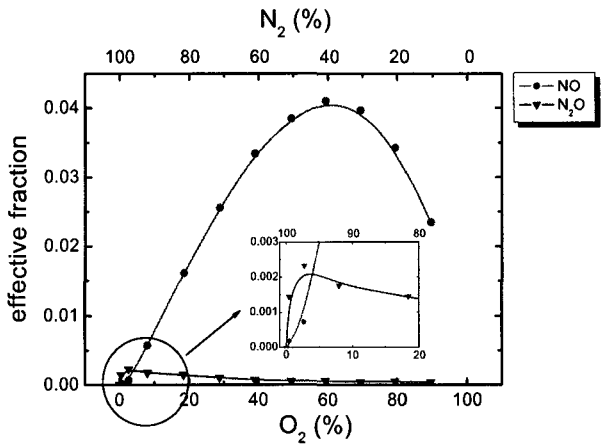

Figure 6.7: NO and N_2O effective fractions are plotted versus the fraction of the admixed O_2 for the mixture measurement at 20 Pa. In the insert the regime at low fractions of the admixed O_2, where the threshold and the N_2O peak are observed, is enlarged.

admixed O_2. In the regime for low fractions of the admixed O_2, the N_2O fraction is also higher than the fraction of NO. Therefore we look in detail to the NO and N_2O fraction for the mixture measurement at 20 Pa from figure 6.4 b). In figure 6.7 the NO and the N_2O fractions are plotted versus the fraction of the admixed O_2. Again the regime for low fractions of the admixed O_2 is blown up in a subfigure in the plot. From this subfigure we can clearly observe that in the regime for low fractions of the admixed O_2, NO shows a threshold behavior and N_2O a maximum.

Finally, we discuss the NO_2 observations. In order to observe the pressure behavior in more detail, the NO_2 effective fractions for all pressures are plotted in figure 6.9. From the plot we can clearly see that the NO_2 fraction decreases with increasing pressure. At 100 Pa it seems that almost no NO_2 is measured at all. It has to be noted here that the signal of NO_2 is almost nearly equal to the detection limit. The final observation we made from figure 6.4 was that at the pressures 9 and 20 Pa NO_2 showed the same trend as NO. In figure 6.10 the fractions for NO and NO_2 are plotted for 9 and 20 Pa logarithmically and we indeed see that NO_2 shows the same trend as NO, except for very low fractions of the admixed O_2. At very low fractions of the admixed O_2 the ratio between NO_2 and NO fractions becomes smaller.

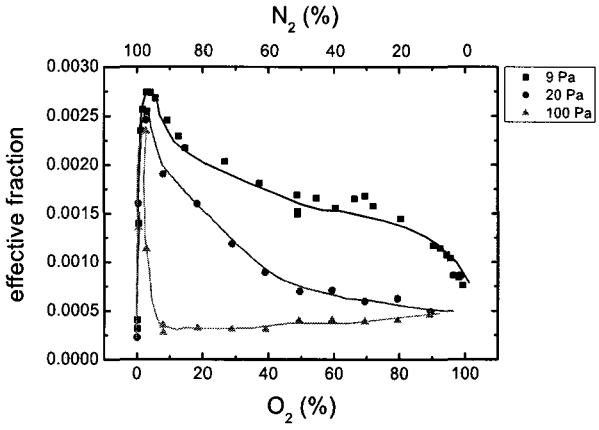

Figure 6.8: In the figure the N_2O fractions are plotted linearly versus the O_2 % for the mixture measurements at 9, 20 and 100 Pa. The N_2O fraction decreases with increasing pressure.

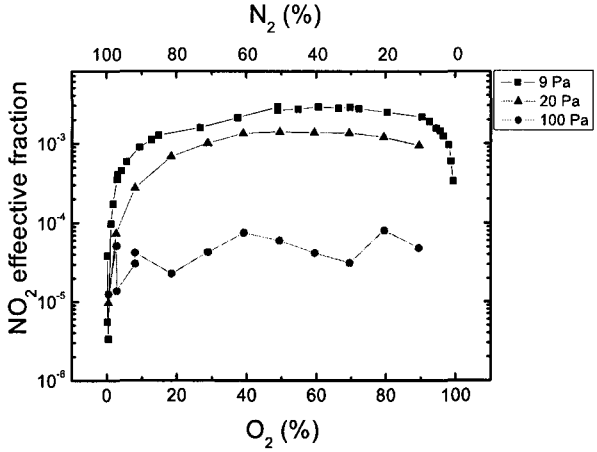

Figure 6.9: The NO_2 fractions for 9, 20 and 100 Pa are plotted linearly versus the fraction of admixed O_2 in order to observe the pressure behavior of NO_2 in more detail. The NO_2 fraction decreases with increasing pressure.

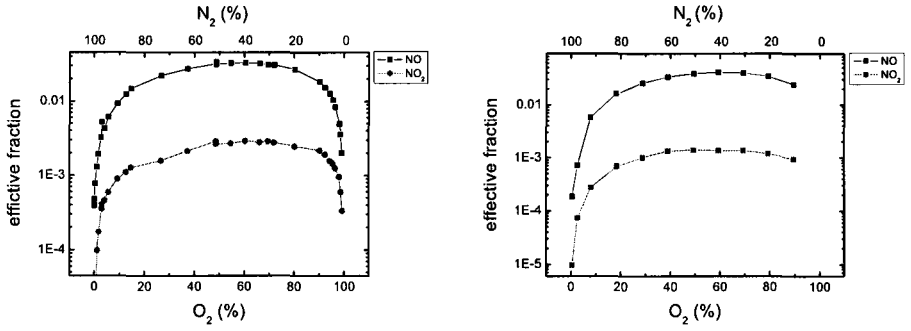

(a) p=9Pa (b) p=20Pa

Figure 6.10: The fractions for NO and NO_2 are plotted for 9 and 20 Pa. The fractions are plotted logarithmical in order to see the trends.

6.3.2 discussion

In this section we discuss the observations made in the previous section. First a set of possible surface reactions and gas phase reactions are given. These reactions are used to discuss the trends for NO, N_2O and NO_2. At the end of the section the conclusions for this section are summarized.

reactions

The following set of gas phase reactions and surface reactions are used to discuss the observations. The rate coefficients and the references are given in appendix A.

$$N \rightarrow N_s \tag{6.12}$$
$$O \rightarrow O_s \tag{6.13}$$
$$N_s + O \rightarrow NO_s \tag{6.14}$$
$$NO_s + N \rightarrow N_2O \tag{6.15}$$
$$N_2O + O \rightarrow NO + NO \tag{6.16}$$
$$N_2O + O \rightarrow N_2 + O_2 \tag{6.17}$$
$$NO_s \rightarrow NO \tag{6.18}$$
$$N + NO \rightarrow N_2 + O \tag{6.19}$$
$$N + O_2 \rightarrow O + NO \tag{6.20}$$
$$NO_s + O \rightarrow NO_2 \tag{6.21}$$

NO threshold

In the regime of low fractions of the admixed O_2 a threshold is observed for the NO effective fraction and a peak for the N_2O effective fraction. A

possible explanation is given for this behavior.

In the explanation the threshold is seen as a quadratic increase of the NO fraction with the admixed O_2. Through reaction 6.14 NO_s is formed at the surface. Because in this regime the N concentration is relatively much higher than the O concentration, most likely all NO_s will be formed into N_2O through reaction 6.15. Then after the threshold NO is formed through reaction 6.16. (At the end of this paragraph this will be shown.) Then the 2-step formation of NO would imply a quadratic behavior with the O concentration. One O atom is needed to form NO_s and one O atom is needed to dissociate N_2O. If reactions 6.14 to 6.16 are added up then reaction 6.22 is found.

$$N_s + N + O + O \rightarrow NO + NO \tag{6.22}$$

It has to be noted that the N concentration practically does not change in this regime of the admixed O_2. Therefore the rate of formation for NO is:

$$\frac{d([NO])}{dt} = k[N]^2[O]^2 \tag{6.23}$$

This reaction has to be integrated over the residence time of the particles. But since the pressure and the total flow are kept constant, the residence time, in equation 2.11 is constant. The N concentration will remain constant for a small variation of the admixed O_2 in this regime. Therefore the NO concentration has a quadratic increase with the admixed O_2 at low fractions of the admixed O_2. This is observed in figure 6.5.

It is noted that the rate for reaction 6.16 is

$$k = 1.5 \cdot 10^{-16} \cdot \exp(\frac{-1.4 \cdot 10^4}{T}) \text{ m}^3\text{s}^{-1} \tag{6.24}$$

and thus this reaction has an activation energy of 1.2 eV. It is also noted that reaction 6.15 is exothermic. The internal energy that a formed N_2O molecule has is then the exothermic energy (Δ E=4.93eV [22]) minus the adsorption energy of NO on the surface and minus the kinetic energy of the desorbed N_2O molecule. One could speculate that the internal energy of a formed N_2O molecule could lead to NO formation through reaction 6.16. Reaction 6.17 has the same activation energy, but different values for the rate coefficient are reported, which indicate that the rate coefficient is a factor of 5 to 40 lower than the rate coefficient for 6.16. That is why this reaction is neglected.

The formation of NO through reaction 6.16 is explained by the rapid decrease of the N_2O effective fraction after the peak. As already mentioned, the N concentration remains practically constant in this regime and therefore only the reaction of N_2O with O remains.

In figure 6.6 the quadratic increase is observed for 20 and 100 Pa. For 9 Pa a linear increase is observed, which can also be seen in figure 6.11

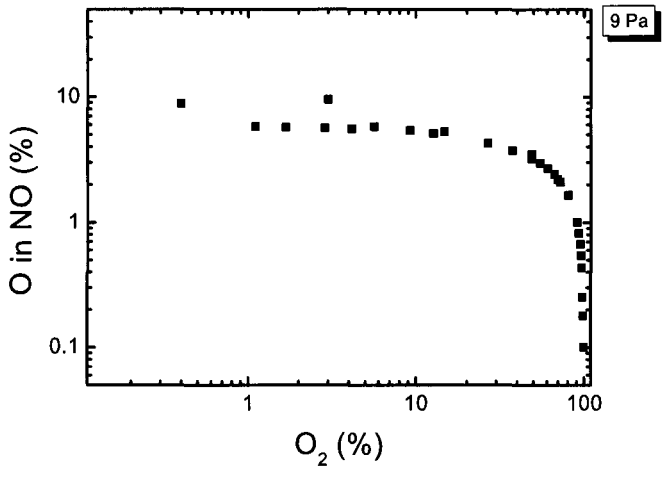

Figure 6.11: For 9 Pa, the atomic fractions of O in NO are plotted. A constant fraction of 5% can be seen up to an admixed O_2 fraction of 20 %.

where the atomic fraction of O in NO is plotted. For higher pressures the dissociation probability of N_2O through reaction 6.16 increases and higher NO effective fractions are expected if the explanation described above is considered. Therefore in the explanation now also reaction 6.19 and 6.20 are suggested. The influence of these gas phase reactions, in this regime of the admixed O_2, seems to decrease for higher pressures resulting in a lower net NO production through these gas phase reactions.

pressure dependence of NO and N_2O effective fractions

In figure 6.8 a decrease is observed after the peak of the effective fraction of N_2O with increasing fraction of the admixed O_2. Furthermore, with increasing pressure this decrease becomes stronger. This pressure dependence can be ascribed to reaction 6.16. Because with increasing pressure the concentrations of O and N_2O increase and therefore the dissociation rate of N_2O. The dependence on the admixed O_2 fraction can also be explained with reaction 6.16, because the O concentration increases. But the main reason is that the NO_s concentration at the surface increases and the concentration of the N radicals decreases. This decreases the probability for an N radical to encounter an NO_s at the surface. Hence reaction 6.18 becomes more favorable then reaction 6.15.

In figure 6.6 it is observed that for fractions higher than 40 % of the admixed O_2, the NO effective fraction increases with increasing pressure. This increase is then most likely caused by reaction 6.20. Another possibility could be that for high pressures NO formation is more favorable than N_2O

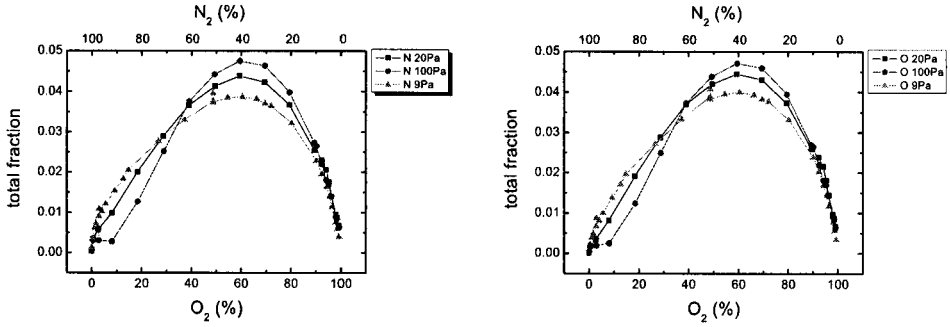

(a) N fraction

(b) O fraction

Figure 6.12: The total fractions of the N and O atoms found in the NO, N_2O and NO_2 molecules are plotted. The total fraction of the N atoms are plotted in a) and the total fraction of O atoms in b).

Table 6.1: Dissociation reactions rate coefficients for NO_2.

reaction		products	k [cm^3/s]
$N+NO_2$	$\rightarrow$	$2O+N_2$	$9.1 \cdot 10^{-13}$
$N+NO_2$	$\rightarrow$	$O+N_2O$	$3 \cdot 10^{-12}$
$N+NO_2$	$\rightarrow$	N_2+O_2	$7 \cdot 10^{-13}$
$N+NO_2$	$\rightarrow$	$NO+NO$	$2.3 \cdot 10^{-12}$
$O+NO_2$	$\rightarrow$	$NO + O_2$	$9.8 \cdot 10^{-11}$

and NO_2. Indeed it is observed that for increasing pressure, the effective N_2O and NO_2 fractions decrease. The atomic fractions of N and O in NO, N_2O and NO_2 should remain constant for varying pressure. From figures 6.12 it is clear that both atomic fractions of N and O are not constant for varying pressure. Although these gas phase reactions cannot be excluded, they are not the main mechanism for the NO increase with increasing pressure.

pressure dependence of NO_2 effective fractions

Finally the NO_2 behavior is discussed. From figure 6.9 a clear pressure dependence is observed and from figure 6.10 the trends of NO and NO_2 are observed to be equal. In table 6.1 the dissociation reactions of NO_2 with their rate coefficients are given [23]. NO_2 is formed by association of NO and O at the surface through reaction 6.21. NO_2 can be dissociated with both N and O radicals in the gas phase.

Conclusions

In this discussion we suggested from the mixture measurement at 20 Pa that NO_s at the surface, which is formed through reaction

$$N_s + O \rightarrow NO_s \tag{6.25}$$

subsequently forms N_2O at low fractions of admixed O_2 through reaction

$$NO_s + N \rightarrow N_2O \tag{6.26}$$

causing the threshold behavior for NO. NO is created through reaction

$$N_2O + O \rightarrow NO + NO \tag{6.27}$$

which causes a quadratic increase of the NO fraction with increasing admixed O_2, which is observed. However, the pressure dependence of NO indicates reaction

$$N + NO \rightarrow N_2 + O \tag{6.28}$$

to be the main responsible reaction causing the threshold behavior for NO.

For fractions higher than 10 %~20 % of the admixed O_2, the formation of NO at the surface through association of N and O and subsequently desorption through reaction

$$NO_s \rightarrow NO \tag{6.29}$$

becomes more favorable instead of N_2O through reaction

$$NO_s + N \rightarrow N_2O \tag{6.30}$$

because the surface concentration of NO increases and the concentration of N decreases.

6.4 Complete conversion of the injected N_2 and O_2 into radicals.

In section 6.3 the conditions of the mixture measurements were chosen in a way that only a fraction of the total injected N_2 and O_2 was dissociated, because the fraction of Ar^+ ions is smaller than the fraction of the injected N_2 + O_2. In section 2 reactions 2.4 to 2.8 are mentioned to be responsible for the creation of radicals. As an example we consider the mixture measurements at 20 Pa and 100 Pa. At an arc current of 75A, 15% of the Ar is ionized. This implies that 0.15 times 3000 sccm = 450 sccm Ar^+ ions are injected. 450 sccm ions can dissociate 450 sccm of the total injected 1900 sccm N_2 + O_2. That would mean that a large fraction of the injected N_2 and O_2 probably does not participate in the reaction mechanism. Besides

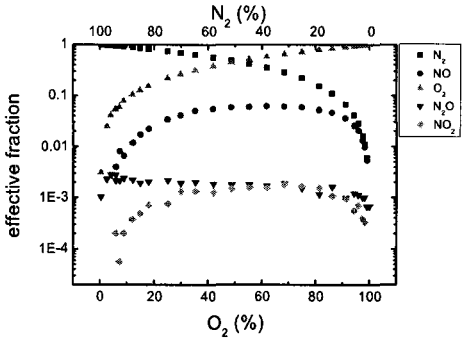

Figure 6.13: Mixture measurements in which all the injected N_2 and O_2 is dissociated. The plasma conditions are: I_{arc}=75 A, p=20 Pa, 5000 sccm Ar, 700 sccm N_2 + O_2 into the background.

it is then not clear what fraction of the N and O radicals recombine to N_2 and O_2. Because the major fraction at the signals for N_2 and O_2 in the mass spectrometer are N_2 and O_2 which is not dissociated.

In this section another mixture measurement is performed in which the conditions are chosen in a way that all the injected gases can be converted into radicals.

6.4.1 Results

The plasma conditions for this measurement are: I_{arc}=75 A, p=20 Pa, 5000 sccm Ar through the Arc, 700 sccm N_2 + O_2 into the background. In figure 6.13 the effective fractions of all molecules are plotted versus the fraction of the admixed O_2. The same trends as for the other mixture measurements are observed. (Keeping in mind that different conditions are used, it is striking that the same amount for the maximum fraction of NO is again found (5%).)

Now in order to see what fraction of radicals end up in which molecule, the atomic fractions are plotted. Because the injected gases are N_2 and O_2, the atomic fractions of N and O are considered. In section 5.2 it was already concluded that the only molecules present in the background are N_2, O_2, NO, N_2O and NO_2. Therefore the atomic fractions of N and O in the molecules N_2, O_2, NO, N_2O and NO_2 are plotted in figure 6.14 and 6.15.

The threshold behavior for NO is seen from the effective fraction in figure 6.13 and from the atomic fraction of N in NO in figure 6.14. From the same figures we also observe that the fractions of NO and NO_2 show the same trend as does the atomic fraction of N in NO and NO_2.

As a last observation it is noted that at high fraction of the admixed O_2 (and thus low fraction of the admixed N_2) up to 30% of all N atoms is found

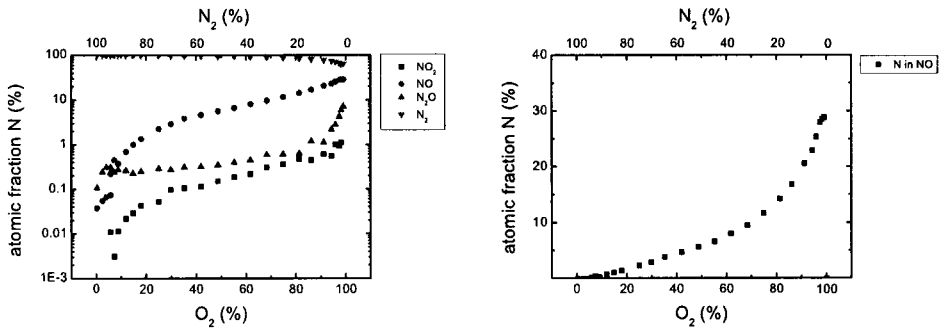

(a) (b)

Figure 6.14: In a) the atomic fractions for N in all molecules are plotted for the mixture measurement in which all injected N_2 and O_2 is dissociated. In b) the atomic fraction of N in NO is plotted given.

in NO.

6.4.2 discussion

The maximum effective NO fraction for the mixture in section 6.3 and the 100% dissociation measurement, is 0.04 respectively 0.06 at 20 Pa, while the injected flows are completely different (I_{arc}=75 A, p=20 Pa, 3000 sccm Ar through the arc and 1900 sccm N_2 + O_2 into the background respectively I_{arc}=75 A, p=20 Pa, 5000 sccm Ar through the arc and 700 sccm N_2 + O_2 into the background). A larger effective fraction is expected, because in this measurement 100% of the injected gases are dissociated, while in the mixture measurement from section 6.3 only 25% is dissociated. Four times more radicals are produced, however the effective fraction is only a factor 1.5 larger.

In figure 6.14 it is seen that at high O_2 %, up to 30% of the available N atoms is found in NO. This implies that NO is efficiently formed. It is assumed that all injected N_2 and O_2 is dissociated. From this observation two statements can be made.

.

NO can be formed in two ways at the surface. An N_s atom at the surface with an O atom from the gas phase or an O_s atom at the surface with an N atom from the gas phase. Because N_2 has a higher binding energy than O_2 (9.76 eV for N_2 and 5.12 eV for O_2) the binding energy of an N atom with the surface is most likely also higher. The NO formed from O_s+N is then assumed to desorb faster than NO formed from N_s+O. Since at high fraction of admixed O_2 the surface will be mainly covered with O atoms and all N radicals will most likely encounter an O atom at the surface to

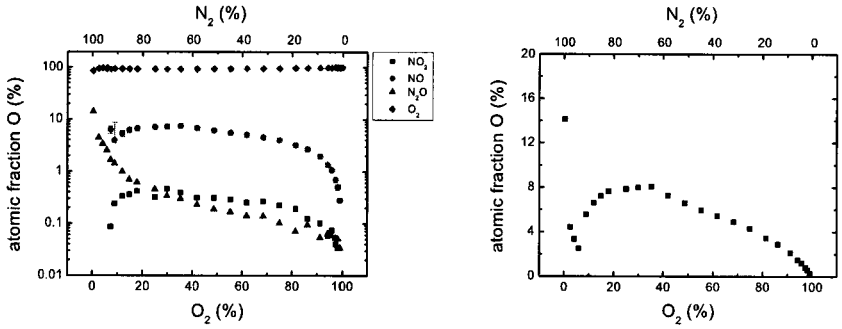

(a) O in all molecules

(b) O in $NO+N_2O+NO_2$

Figure 6.15: In a) the atomic fractions for O in all molecules are plotted for the mixture measurement in which all injected N_2 and O_2 is dissociated. In b) the atomic fraction of O in $NO+N_2O+NO_2$ is plotted.

form NO and subsequently desorb. The effective NO formation could be a consequence of this high NO surface coverage and if so, this would imply a direct desorption of NO from the surface.

More likely is an explanation with the gas phase reactions:

$$N + O_2 \rightarrow NO + O \quad (6.31)$$

$$N + NO \rightarrow N_2 + O \quad (6.32)$$

At high fractions of the admixed O_2, the probability of N to encounter O_2 in the gas phase is high, causing efficient formation of NO through reaction 6.31. And because the concentration of NO is low in this regime (and keeping in mind that N is efficiently used in reaction 6.31), nearly no NO is dissociated through reaction 6.32. Besides this, extra O radicals are created. These radicals can reach the surface, which can lead to NO production at the surface.

Furthermore at low admixed fractions of O_2, up to 15% of the O atoms can be found in N_2O. This supports the statement on the formation of N_2O in the low O_2 % regime. The surface concentration of N is much higher than the surface concentration of O, because almost all injected gas is N_2 with a small fraction of O_2. Therefore the radicals are mainly N radicals. The O radicals have a large chance to encounter an N radical at the surface to form NO_s. This NO_s molecule at the surface has a high probability to encounter another N radical to form N_2O. Because of the high probability for an O to encounter a N radical at the surface and the high probability for NO at the surface to encounter an N radical, we directly assume that N_2O is efficiently formed from the available O radicals.

6.4.3 conclusions

For a plasma conditions in which all injected molecules are converted into radicals, nearly the same effective fractions are measured as for plasma conditions in which only a fraction of the injected molecules are converted into radicals.

At high fractions of the admixed O_2, NO is efficiently formed, at the surface, most likely through reaction

$$N + O_s \rightarrow NO \tag{6.33}$$

or in the gas phase, most likely through reaction

$$N + O_2 \rightarrow NO + O \tag{6.34}$$

At low fractions, N_2O is efficiently formed, most likely at the surface through reaction

$$NO_s + N \rightarrow N_2O \tag{6.35}$$

6.5 Pressure dependence of the formation and dissociation of NO, N_2O and NO_2.

In the previous section, mixture measurements at 3 different pressures were discussed for the NO, N_2O and NO_2 effective fractions. In this section the pressure dependencies will be discussed in more detail, by showing measurements in which the pressure is varied over a wide range from 4 Pa to 350 Pa. The injected gas flows are taken constant during these measurements and chosen in a way that the maximum NO effective fraction is measured. In the previous measurements the maximum was found to be at 60 % of the admixed O_2 for the mixture measurements at 9, 20 and 100 Pa (see figure 6.6). The total flow is chosen in a way that the injected N_2 and O_2 are completely converted into radicals. The plasma conditions are: I_{arc}=75 A, p=20 Pa, 5000 sccm Ar, 280 sccm N_2 and 420 sccm O_2 into the background. At 75 A, 15 % of the flow through the arc is ionized. Then a flow of 750 sccm Ar^+ is created, which is more than the total of 600 sccm injected in the background. Hence all the injected gases in the background are converted into radicals under these conditions.

6.5.1 Results and discussion

In figure 6.16 the partial pressure and the effective fraction of NO_2 are plotted. The partial pressure shows a maximum around a pressure of 15 Pa. However, the effective fraction shows an exponential decrease.

In figure 6.9 it is observed that at 100 Pa hardly any NO_2 is present. Also for the present conditions, the NO_2 values are small for high pressures

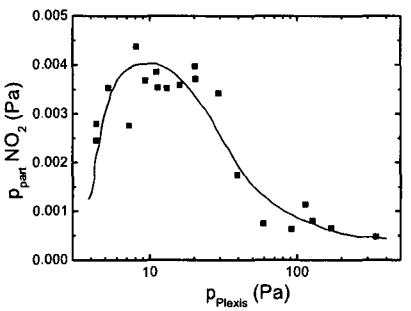

(a) NO_2 partial pressure

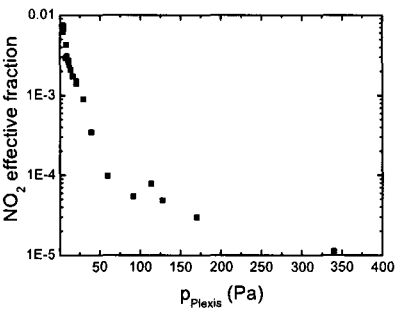

(b) NO_2 fraction

Figure 6.16: In a) the partial pressure for NO_2 with a guide to the eye, and in b) the effective fraction for NO_2 versus the total pressure are plotted. The plasma conditions are: I_{arc}=75A, 5000 sccm through the arc, 280 sccm N_2 and 420 sccm O_2 in the background.

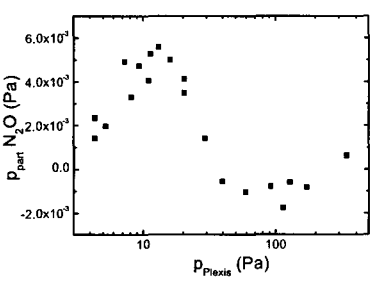

(a) N_2O pressure

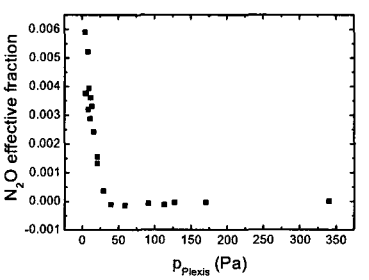

(b) N_2O fraction

Figure 6.17: In a) the partial pressure for N_2O and in b) the effective fraction for N_2O versus the total pressure are plotted. The plasma conditions are: I_{arc}=75A, 5000 sccm through the arc, 280 sccm N_2 and 420 sccm O_2 in the background.

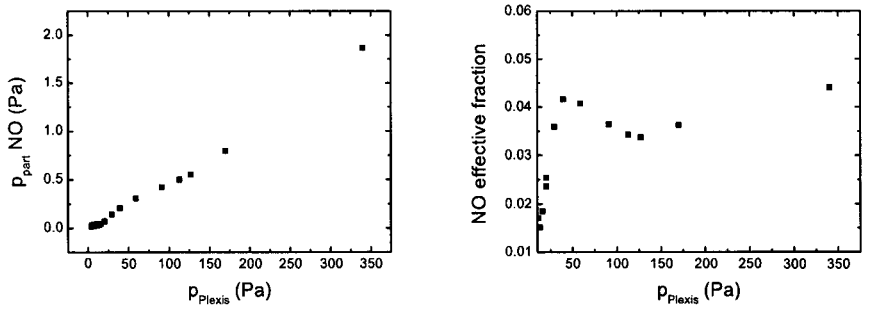

(a) NO partial pressure

(b) NO fraction

Figure 6.18: In a) the partial pressure of NO and in b) the effective fraction of NO versus the total pressure are plotted. The plasma conditions are: I_{arc}=75A, 5000 sccm through the arc, 280 sccm N_2 and 420 sccm O_2 in the background.

(p > 100 Pa) as shown in figure 6.16. The dissociation reactions with N and O, which are already proposed in table 6.1 in the previous section, are most likely responsible for the decrease of the effective fraction with increasing pressure.

In figure 6.17 the same trends for the N_2O pressure dependence is observed as for NO_2. The decrease of the effective fraction for N_2O is most likely caused by the dissociation reaction of N_2O with O.

In figure 6.18 the partial pressure and fraction of NO are plotted versus the total pressure. The partial pressure of NO shows a linear behavior with pressure. Figure 6.18b) shows an increasing NO effective fraction with increasing pressure.

6.6 Maximum conversion calculations

In the discussion in section 6.3.2 it is suggested that in the regime of low fractions of admixed O_2, efficiently N_2O is formed. In this section a model is proposed to calculate the maximum N_2O effective fraction. In this model the following assumptions are made for the calculation.

1. Every Ar^+ ion dissociates a molecule.
2. The production of N and O radicals occurs via Ar^+ ions.
3. Only N_2, O_2 and N_2O are formed
4. From the radicals created, the maximum possible N_2O is formed.
5. Production of radicals through gas phase reactions are neglected.

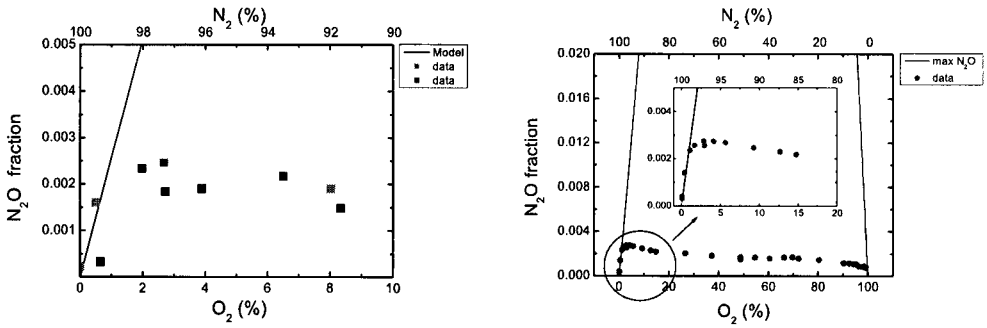

(a) 20 Pa (b) 9 Pa

Figure 6.19: The maximum calculated N_2O effective fraction is plotted together with data from mixture measurements with the same conditions used for the calculation. In a) the plasma conditions are: 3000 sccm Ar through the arc, I_{arc}=75 A, p = 20 Pa and 1900 sccm N_2 + O_2 into the background. In b) the plasma conditions are: 1500 sccm Ar through the arc, I_{arc}=75 A, p = 9 Pa and 900 sccm N_2 + O_2 into the background.

The surface coverage, suggested for low fractions of the admixed O_2, implies an efficient N_2O formation, which is also seen and concluded in section 6.4. Comparing the model with the data could support the suggested surface coverage.

Now an overview of the calculation of the maximum effective N_2O fraction will be given for an Ar flow of 3000 sccm through the arc, an arc current of 75 A, 900 sccm N_2 and 900 sccm O_2. The Ar^+ ion flow is 450 sccm, which means that 450 sccm N_2 + O_2 is dissociated. The ratio of dissociation is of N_2 and O_2 is assumed to be 2 (considering ratio of the rate of the charge transfer reactions for N_2 and O_2, see appendix A) and determines in which ratio the N_2 and O_2 molecules dissociate. 300 sccm N_2 and 150 sccm O_2 can be dissociated, creating 600 N sccm radicals and 300 O sccm radicals. The maximum possible N_2O is then 300 sccm. Dividing this by the total flow gives the effective fraction.

Results and discussion

For the plasma conditions the conditions for the mixture measurements at 9 and 20 Pa from section 6.3 are taken. In figures 6.19 the maximum possible N_2O effective fraction is plotted with the data for N_2O effective fractions at 20 and 9 Pa. From the enlarged plot in the inset in figure 6.19b) a good agreement is seen between the calculated maximum and the data at low fractions of the admixed O_2.

At low fractions of the admixed O_2 the calculated maximum N_2O fraction

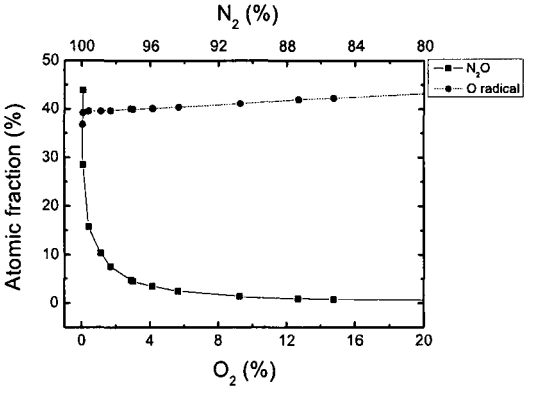

Figure 6.20: For the mixture measurement at 9 Pa the atomic fractions of O in N_2O is plotted. The fraction of O_2, which is dissociated, is also plotted. The plasma conditions are: 1500 sccm Ar through the arc, I_{arc}=75 A, 900 sccm N_2 + O_2 into the background.

is nearly equal to the measured N_2O fraction. This means that N_2O is efficiently formed in the low O_2 % regime. This supports our statement that in the regime of low admixed O_2 the surface coverage will consist of mainly N and some NO. Every NO on the surface will most likely react with an N radical to form N_2O. Finally in figure 6.20 the atomic fraction of O in N_2O is compared with the fraction of O_2 which is dissociated for the given conditions (assuming no O radicals are lost). From the figure it is observed that at low fractions of the admixed O_2, nearly all created O radicals are found in N_2O.

6.7 Equilibrium of formation and dissociation

Until now the maximum NO effective fraction was found to be 4±2 % for measurements with different plasma conditions in which an equal amount for N_2 and O_2 are injected into the background. (See as examples figures 6.6 and 6.13) As a possible explanation, an equilibrium between formation reactions and dissociation reactions of NO is proposed. To investigate this, in this section the amount of radicals created in a measurement will be compared with the amount of radicals measured in the molecules NO, N_2O and NO_2.

6.7.1 Results and discussion

In this section the atomic fractions of N and O in the molecules NO, N_2O and NO_2 are compared with the fraction of the created radicals for 2 mea-

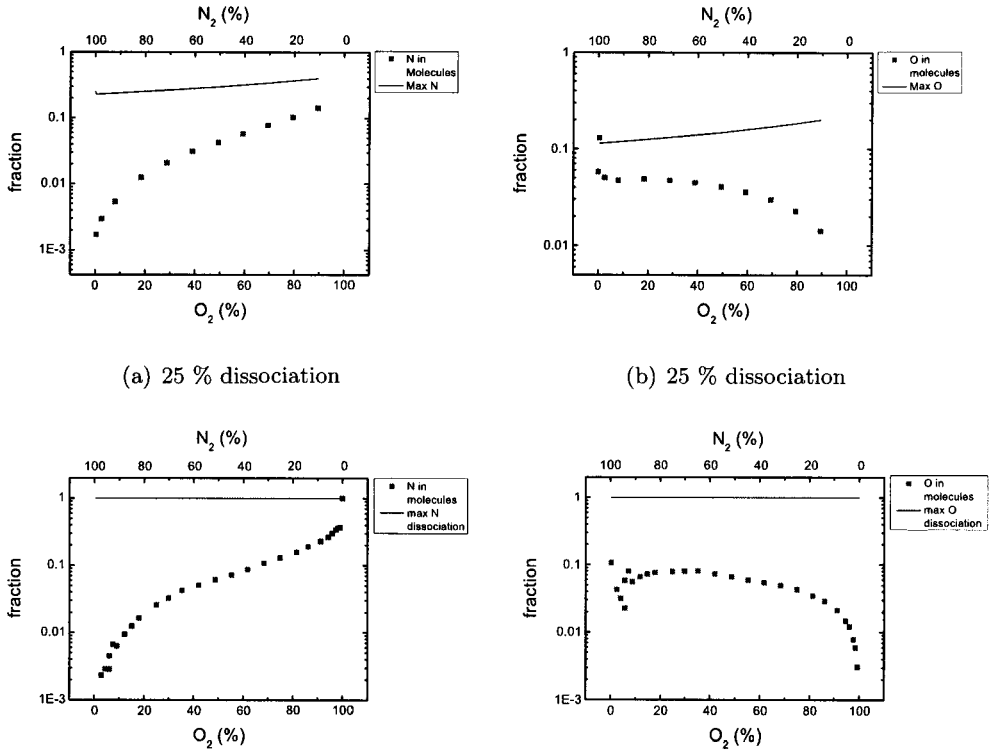

(a) 25 % dissociation

(b) 25 % dissociation

(c) Full dissociation

(d) Full dissociation

Figure 6.21: In the figures the dissociated fractions of N_2 and O_2 are given together with the fractions of the N or O atom which is found back in NO, $N_2O$and NO_2.

surements. In figure 6.21a) and b) the mixture measurement, in which 25 % of the injected N_2 and O_2 can be converted into radicals, is plotted. The plasma conditions are: I_{arc}=75 A, 3000 sccm Ar through the Arc, 1900 sccm N_2 + O_2 into the background and p = 20 Pa.

In figure 6.21c) and d) the mixture measurement, in which 100 % of the injected N_2 and O_2 can be converted into radicals, is plotted. The plasma conditions are: I_{arc}=75 A, p=20 Pa, 5000 sccm Ar through the arc, 700 sccm N_2 + O_2 into the background.

In figure 6.21a) and b) a higher fraction of the radicals is found back in the molecules than in figure 6.21c) and d).

At a higher conversion fractions, the amount reactive species is higher. Therefore a larger fraction of molecules can formed. Therefore higher atomic fraction of the radicals in the molecules are expected at a conversion fraction of 100%. But the opposite is observed. Therefore this observation makes it more plausible that the NO fraction is determined by formation

and dissociation reactions.

6.8 Conclusions

The goal of this research is determining the generation of molecules in N_2/O_2 plasmas. Stable molecules were measured in the background of an expanding thermal plasma by means of mass spectrometry.

From mixture measurements at several pressures, in which the admixed O_2 % is varied, a threshold behavior is found for NO at low fractions of the admixed O_2. In a first explanation NO is created at the surface, through reaction

$$N_s + O \rightarrow NO_s \tag{6.36}$$

Subsequently N_2O is formed through reaction

$$NO_s + N \rightarrow N_2O \tag{6.37}$$

If only the O density is large enough, above the threshold, NO can be formed from N_2O by the reaction:

$$N_2O + O \rightarrow NO + NO \tag{6.38}$$

This gives a quadratic increase with O density, which would thus explain the threshold behavior.

It is concluded from the measurements that not only surface reactions, but also gas phase reactions play a role in the formation and destruction of NO. NO can be formed by the reaction

$$N + O_2 \rightarrow O + NO \tag{6.39}$$

as was earlier concluded by van Helden [11]. The O radical can subsequently be used at the surface to form a second NO molecule, which desorbs:

$$N + O_s \rightarrow NO_s \tag{6.40}$$

Gas phase reactions lead also to the loss of NO:

$$N + NO \rightarrow N_2 + O \tag{6.41}$$

Again the O radical formed in this reaction can adsorb at the surface and lead there to new molecules. As both production and destruction of NO molecules are thus caused by N atoms, the resulting fraction would be determined by the balance of these processes.

It is noted that reactions 6.39 and 6.41 are an extra source of O radical production, next to charge transfer and subsequently dissociative recombination. In this explanation, volume and surface reactions play a role in the

NO formation. That the surface plays a role is indicated by the quadratic increase of NO with the injected O_2 fraction and by the dominance of N_2O formed at low O fractions.

Also the pure surface association of N and O radicals plays a role, like the formation of N_2 molecules in pure N_2 plasmas and O_2 molecules in pure O_2 plasmas. In this case the following reactions prevail:

$$O \rightarrow O_s \tag{6.42}$$

$$N \rightarrow N_s \tag{6.43}$$

It is also likely that NO_2 is formed at the surface by the reactions

$$O + NO_s \rightarrow NO_2 \tag{6.44}$$

$$NO + O_s \rightarrow NO_2 \tag{6.45}$$

NO_2 is subsequently converted to other molecules by the reactions:

$$NO_2 + N \rightarrow NO + NO \tag{6.46}$$

$$NO_2 + N \rightarrow N_2 + O_2 \tag{6.47}$$

$$NO_2 + N \rightarrow N_2O + O \tag{6.48}$$

$$NO_2 + O \rightarrow NO + O_2 \tag{6.49}$$

It could probably be a clue for the fact that the dependence of NO_2 on the admixed O_2 fraction is very similar to the NO dependence.

For a more detailed picture of molecule formation, the relative use of either O or N radicals for the formation of molecules is investigated at low fractions of O_2 or N_2 admixture.

For low fractions of admixed O_2, up to 15% of the formed O radicals is found back in N_2O (and practically none in NO). This can be explained in a picture in which the surface is mainly covered by N and NO radicals, as indicated before.

For fractions higher than 10% of the admixed O_2 mainly NO is observed. Apparently, enough O radicals are present to convert N_2O to NO and also NO can be formed directly at the surface.

At low fractions of N_2 (thus even higher fractions of O_2) it appears that NO is efficiently formed. Up to 30% of the N radicals is found back in NO. Now the surface is probably mainly covered by O atoms and NO can be formed efficiently by association to N atoms at the surface. Also the gas phase reaction 6.39 can give rise to efficient formation of NO.

For nearly all measurements with different conditions the effective fraction for NO is constant (4±2 %). This could indicate that the formation of NO is determined by a balance of N induced production and destruction processes. It is evident thus that for NO formation gas phase reactions are

important; likewise surface reactions are important as well as is also clear from the N_2O and NO_2 formation. It thus proves that quantative mass spectrometry is a very suitable methodology to obtain the absolute densities of molecules and therewith an indication of the processes important for the production of molecules in a plasma.

Chapter 7

Conclusions

The goal of this research is determining the formation of molecules in N_2/O_2 plasmas. By measuring the concentrations of stable molecules using mass spectrometry, pathways for formation of the molecules have been deduced. A calibration procedure for mass spectrometry has been presented with which absolute concentrations can be obtained. The concentrations achieved with this procedure showed agreement within 10% of the concentrations measured with absorption spectroscopy.

Mass scans with a mass spectrometer showed that in an N_2/O_2 plasma besides Ar, N_2 and O_2 molecules, also NO, N_2O and NO_2 are detected.

From mixture measurements at several pressures, several reactions were found to be important for the formation of NO. NO is formed at the surface through association of N and O radicals. NO can be formed in the gas phase, through dissociation of N_2O with O in the gas phase giving NO als a product. NO can also be formed in the gas phase by a reaction of N and O_2, producing an extra O radical next to NO. In the gas phase, NO can be dissociated with an N radical to form N_2 and an O radical. Therefore, both gas phase reactions are an extra mechanism for O radical creation, next to charge transfer of N_2 and O_2 with Ar^+ ions and subsequently dissociative recombination.

N_2O formation occurs at the surface. Dissociation in the gas phase results in production of NO. At low fractions of the O_2, N_2O is efficiently formed. For higher fractions however, this efficiency decreases, because the surface coverage changes and formation of NO becomes more favorable. Moreover, due to a higher O concentration, the rate of dissociation of N_2O with O in the gas phase increases.

At constant pressures (< 30 Pa) a constant ratio between NO_2 and NO is found for different mixtures of N_2 and O_2. The reasons for this behavior is not clear as yet. We can remark that NO_2 must be formed at the surface by association of NO and O radicals. Furthermore, it is noted that NO_2 is easily dissociated with an N or O radical. Therefore only low concentrations

are measured compared to NO and N_2O.

For nearly all measurements with different conditions the effective fraction for NO is constant (4±2 %). This implies the reaction mechanism for the formation of NO is determined by a balance in a set of gas phase reactions and dissociation reactions.

These reactions can be used as input of a model in future research for these type of plasmas. For this model, the rate coefficients for the surface reactions have to be determined. The surface coverage needs to be known in more detail. Accurate temperature measurements are needed in the process chamber and the recirculation needs to be investigated.

Chapter 8

Word of Thanks

I would like to thank first of all, my parents and my sister for supporting me during my graduation project.

Many thanks are for Rens, my supervisor. He has helped me during my whole graduation period and has given me many good advices. He has taught me how to keep everything ordered and kept me focused and therefore, with his efforts I have learned to work more efficiently. I also like to thank my other supervisor Richard Engeln. He too has taught me to work efficiently and ordered. And last, but certainly not least, as my supervisors, I would like to thank my graduation professor, Daan Schram. He has given me much insight in the plasma physics (I could not always immediately figure out what he was saying, but eventually I did).

Their supervision has made me analyze my data more critically and work more efficiently amongst others, which have finally led to my graduation thesis.

Furthermore, I would like to thank everybody who helped in anyway for my graduation, especially Jean-Pierre. Our discussions concerning my subject of graduation enlightened me (I hope him too) in many cases. I would like to thank Ries for helping me build and repairing my setup. I also like to thank Bertus, for making a safety device for my setup, which turned out to be very useful, and Jo, Herman and Janneke for their help.

I would like to thank all members of the ETP Darts Federation, which is everyone who has ever thrown a dart in the student room. Especially Paul for lending his darts board and thereby initiating the foundation of the dart competition. I have discovered that darts can be a very welcome distraction when writing your thesis until 12 o'clock in the night in the student room.

I have had many laughs with everyone, moreover I would like to thank the other 50% of the Turkish delegation at ETP, Kerim, for having typical turkish "geyik" conversations. I always enjoyed to watch and support our soccer team PEST. I hope the PEST "scandal", discovered by me, did not

cause Bram and Stephan too much problems. I also like to thank Bram for his support during "heavy" times, that is, when we were lifting weights.

If I have forgotten someone to thank, who feels that he or she should be thanked too, then he or she can consider him or herself thanked by me. Finally I would like to say, that I enjoyed doing my graduation at ETP. The group has a great atmosphere and therefore made working there very pleasant.

Bibliography

[1] J.E. Crowell, J. Vac. Sci. Technol. A **21**, S88 (2003)

[2] H.J.N. van Eck, A. den Ouden, G.J. van Rooij, W.J. Goedheer, B. de Groot, N.J. Lopes Cardozo and A.W. Kleyn, IEEE transactions on applied superconductivity **15**, 1303 (2005)

[3] N. Philip, IEEE Transactions on Plasma Science **30**, 1429 (2002)

[4] M. Bradford, R. Grover, P. Pau, Chem. Eng. Prog. **98**, 38 (2002)

[5] X. Hu, Fuel **82**, 1675 (2003)

[6] M. Baeva, H. Gier, A. Pott, J. Uhlenbusch, J. Höschele, and J. Steinwandel, Plasma Chemistry and Plasma Processing **21**, 225 (2001)

[7] M.C.M. van de Sanden, R.J. Severens, W.M.M. Kessels, R.F.G. Meulenbroeks, and D.C. Schram, J. Appl. Phys. **84**, 2426 (1998)

[8] M.A. Blauw, private communication

[9] Visual DSMC Program for Two-Dimensional and Axially Symmetric Flows, Version 3.1, March 2005

[10] J. Röpcke, L. Mechold, M. Käning, J. Anders, F.G. Wienhold, D. Nelso, and M. Zahniser, Rev. Sci. Instrum. **71**, 3706 (2000)

[11] J.H. van Helden, The generation of molecules through plasma-surface interactions, PhD thesis, Eindhoven University of Technology, Eindhoven, (2006)

[12] E. Kieft, Mass spectrometry and ex-situ ellipsometry as analysis tools for plasma enhanced deposition of ZnO thin films, master thesis, Eindhoven University of Technology, Eindhoven, 2001

[13] W. Wagemans, Infrared spectroscopy and mass spectrometry on ammonia formed in N_2-H_2 plasma, internal report, Eindhoven University of Technology, Eindhoven, October 2002

[14] J.M. Austin, and A.L.S. Smith, J. Phys. D: Appl. Phys. **6**, 2236 (1973)

[15] M. Hawley, M.A. Smith, J. Phys. Chem. **96**, 6693 (1992)

[16] A. Nerken et. al., J. Vac. Sci. **9**, 1260 (1972)

[17] G.J.H. Brussaard, K.G.Y. Letourneur, M. Schaepkens, M.C.M. van de Sanden, and D.C. Schram J.Vac. Sci. Technol. **21**, 62 (2003)

[18] J.H. van Helden, R. Zijlmans, R. Engeln, and D.C. Schram, IEEE Transactions on Plasma Science **33**, 390 (2005)

[19] E. Murad, Annu. Rev. Phys. Chem. **49**, 73 (1998)

[20] H. Singh, J.W. Coburn, and D.B. Graves, Journal of Applied physics **88**, 3748 (2000)

[21] B Gordiets, J. Phys. D: Appl. Phys. **29**, 1021 (1996)

[22] M. Capitelli, C.M. Ferreira, B.F. Gordiets, and A.I. Osipov, Plasma kinetics in atmospheric gases, Springer-Verlag, Berlin (2000)

[23] I.A. Kossyi, A.Y. Kostinski, A.A. Matveyev, and V.P. Silakov, Plasma Sources Sci. Technol. **1**, 207 (1992)

[24] G.J.H. Brussaard, Remote arc generated plasma in diatomic gases, PhD thesis, Eindhoven University of Technology, Eindhoven, (1999)

[25] S.C. Brown, Basic data of plasma physics, 2nd ed. (MIT, Cambridge, MA, 1996).

[26] J.B. Hasted, Physics of atomic collisions, 2nd ed. (Butterworths, London, 1972)

[27] J.B. Hasted, Physics of atomic collisions, 2nd ed. (Butterworths, Washington DC, 1964)

[28] L.F. Philips and H.I. Schiff, J. Chem. Phys. **42**, 3171 (1965)

Appendix A

Rate of gas phase reactions

In table 8.1, all the rate coefficients of the gas phase reactions used in this report are given in Arrhenius form. For each reaction the reference is also shown. Note that the charge transfer reactions, dissociative recombination reactions and the dissociation reactions of NO_2 have no temperature dependence.

Table 8.1: Rate coefficients for gas phase reactions in Arrhenius form.

reactants		products	rate coefficient [m^3/s]	reference
$Ar^+ + N_2$	$\rightarrow$	$N_2^+ + Ar$	$2 \cdot 10^{-16}$	[24]
$Ar^+ + O_2$	$\rightarrow$	$O_2^+ + Ar$	10^{-16}	[25] [15]
$N_2^+ + e^-$	$\rightarrow$	$N^* + N$	10^{-13}	[26]
$O_2^+ + e^-$	$\rightarrow$	$O^* + O$	10^{-13}	[27]
$N_2O + O$	$\rightarrow$	$NO + NO$	$1.5 \cdot 10^{-16} \exp(-1.4 \cdot 10^4/T)$	[22]
$N_2O + O$	$\rightarrow$	$N_2 + O_2$	$(0.4\text{-}3) \cdot 10^{-17} \exp(-1.4 \cdot 10^4/T)$	
$N + O_2$	$\rightarrow$	$NO + O$	$3.2 \cdot 10^{-18}\ (T/300) \exp(-3150/T)$	[23]
$N + NO$	$\rightarrow$	$N_2 + O$	$1 \cdot 10^{-18}\ T^{0.5}$	[23]
$N + NO_2$	$\rightarrow$	$2O + N_2$	$9.1 \cdot 10^{-19}$	[23] [28]
$N + NO_2$	$\rightarrow$	$O + N_2O$	$3 \cdot 10^{-18}$	[23] [28]
$N + NO_2$	$\rightarrow$	$N_2 + O_2$	$7 \cdot 10^{-19}$	[23] [28]
$N + NO_2$	$\rightarrow$	$NO + NO$	$2.3 \cdot 10^{-18}$	[23] [28]
$O + NO_2$	$\rightarrow$	$NO + O_2$	$9.8 \cdot 10^{-17}$	[23] [28]

Appendix B

Ar/He measurements

In this section mixture measurements are performed in which a mixture of Ar and He is fed through the arc. By doing this, the average mean free path is reduced compared to when an Ar arc is used. Because the atomic mass of He is 2 and of Ar is 40. The average mass is therefore smaller when an Ar/He arc is used than when an Ar arc is used, hence the average mean free path is smaller. By doing so, the dissociation of NO through gas phase reactions can be investigated.

results

Four measurements have been performed at pressures of 5.8 to 13 Pa. The plasma conditions are given in the figures 8.1 and their conditions are given in table 8.2.

Comparison of these figures with each other shows that the effective fraction for NO clearly increases with decreasing pressure, especially for fractions of the admixed O_2 up to 40%. At a fraction of the admixed O_2 of 6%, a value of 2% is observed for the effective NO fraction. Furthermore, the maximum effective fraction for NO is found at approximately at 20%.

Finally in figure 8.2 the effective NO fractions are plotted for all pressures.

Table 8.2: conditions for the Ar He measurements

figure	Ar flow (arc) [sccm]	He flow (arc) [sccm]	N_2+O_2 flow (bg.) [sccm]	pressure [Pa]
8.1a)	300 sccm	1500	200	5.8
8.1b)	600 sccm	3000	200	11.9
8.1c)	600 sccm	3000	600	12.7
8.1d)	600 sccm	3000	1000	13.3

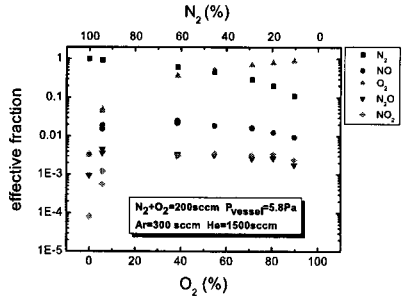

(a) p = 5.8 Pa

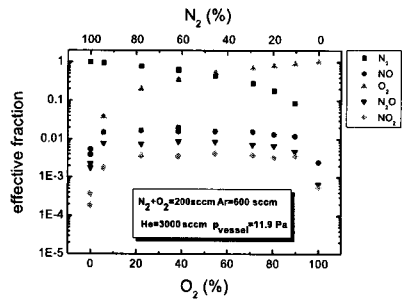

(b) p = 11.9 Pa

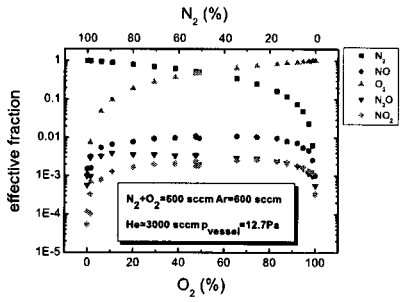

(c) p = 12.7 Pa

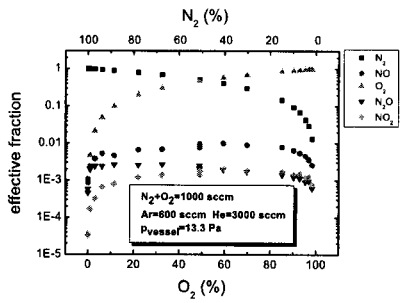

(d) p = 13.3 Pa

Figure 8.1: Ar/He measurements

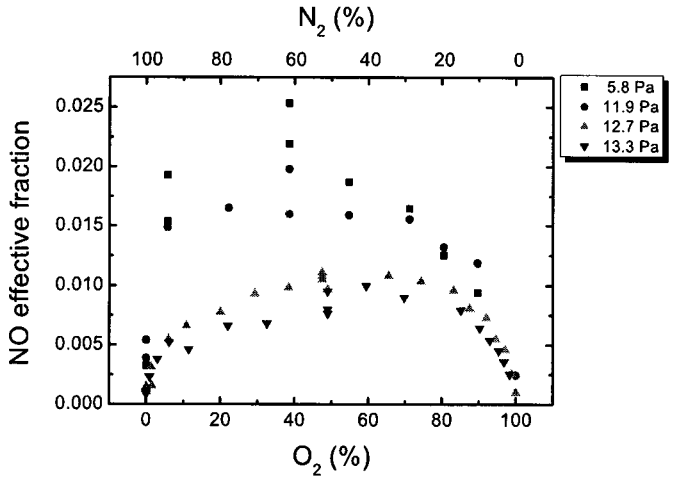

Figure 8.2: The NO effective fractions for all conditions

discussion

For the discussion first the set of reactions, responsible for the formation and dissociation of NO in the gas phase and at the surface, are considered again.

$$N_2O + O \rightarrow NO + NO \quad (8.1)$$
$$NO_s \rightarrow NO \quad (8.2)$$
$$N + NO \rightarrow N_2 + O \quad (8.3)$$
$$N + O_2 \rightarrow O + NO \quad (8.4)$$

Furthermore it is noted that helium has a much higher ionization energy than argon. Therefore it is assumed that in figures 8.1a) to b), more Ar^+ ions are created then N_2 and O_2 are injected. The injected N_2 and O_2 are assumed to be fully converted into radicals in these measurements.

First the difference in NO for 5.8 Pa and 11.9 Pa is discussed. The residence time for both conditions is equal. The mean free path is for the condition at 5.8 Pa larger. So with a lower pressure and a higher mean free path more NO is measured. The contribution of the surface for the NO formation is assumed to be constant. If only reaction 8.4 is considered, less NO is expected for lower pressures and larger mean free path. Hence reaction 8.3 has to be taken into account. A lower pressure and larger mean free path implies a smaller dissociation probability of NO through reaction 8.3 and hence more NO is measured.

Comparison with the pressure measurements in section 6.5, in which the fractions of the admixed O_2 is 60%, points out that the effective fraction of NO is 1.8% around 12 Pa for the Ar arc case and 1.6% for the Ar/He arc case. The residence time for both conditions is equal and in both conditions the injected N_2 and O_2 can be fully converted. This implies that mean free path does not have a significant influence on the net formation of NO for the same pressures.

Finally it is noted that if the atomic fraction of O in NO is considered (figure 8.3), up to 25% of the injected O_2 is found back in NO at low fractions of the admixed O_2.

conclusions

The increase of the effective fraction of NO, when the pressure is decreased from 10 Pa to 5.8 Pa, can be ascribed to a set of reactions including formation and dissociation reactions of NO in the gas phase and formation reactions

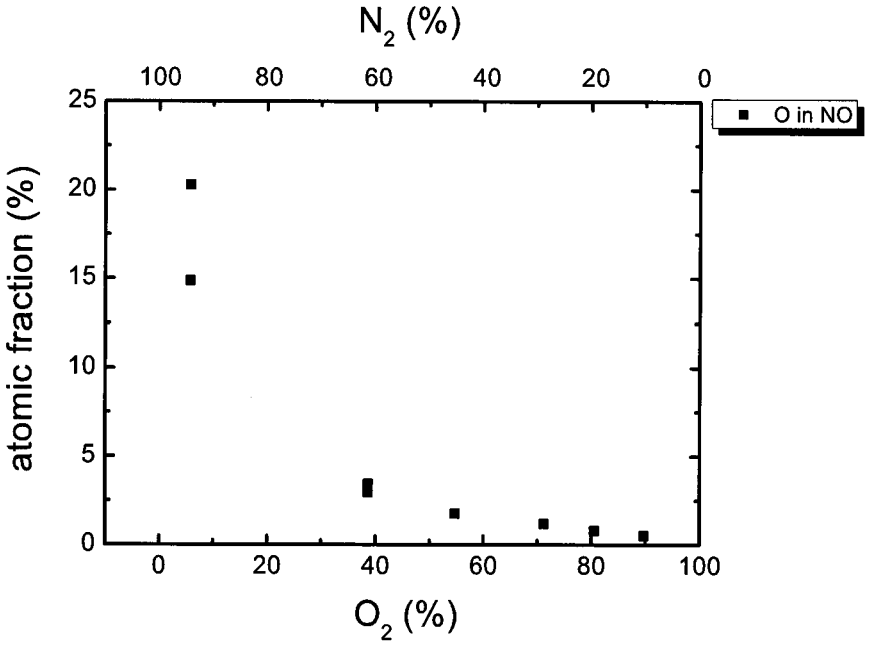

Figure 8.3: Atomic fraction of O in NO at 5.8 Pa.

of NO at the surface. (reactions 8.5 to 8.8)

$$N_2O + O \rightarrow NO + NO \tag{8.5}$$
$$NO_s \rightarrow NO \tag{8.6}$$
$$N + NO \rightarrow N_2 + O \tag{8.7}$$
$$N + O_2 \rightarrow O + NO \tag{8.8}$$

Varying the mean free path for the same pressures does not have a significant influence on the net formation of NO .